Coordination Chemistry Reviews 437 (2021) 213713

Contents lists available at ScienceDirect

Coordination Chemistry Reviews

journal homepage: www.elsevier.com/locate/ccr

Review

1,8-Naphthalimide based fluorescent sensors for enzymes

Conor Geraghty [a,b,c,1], Conor Wynne [a,b,1], Robert B.P. Elmes [a,b,c,*]

[a] Department of Chemistry, Maynooth University, National University of Ireland, Maynooth, Co. Kildare, Ireland
[b] Synthesis and Solid-State Pharmaceutical Centre (SSPC), Maynooth University, National University of Ireland, Maynooth, Co. Kildare, Ireland
[c] Kathleen Lonsdale Institute for Human Health Research, Maynooth University, National University of Ireland, Maynooth, Co. Kildare, Ireland

ARTICLE INFO

Article history:
Received 31 August 2020
Received in revised form 6 November 2020
Accepted 8 November 2020
Available online 20 March 2021

Keywords:
1,8-Naphthalimide
Enzyme activation
Fluorescent sensors
Fluorescent probes
Biomarker detection
Cellular imaging
Diagnostics

ABSTRACT

Fluorescent probes have long been valuable tools in the study of biological systems. With the ever-expanding range of known enzymatic biomarkers for disease, it has never been more important to develop synthetically facile, sensitive, selective, and robust methods for the detection of these analytes. The 1,8-naphthalimide fluorophore presents an ideal scaffold on which to design a range of fluorescent probes for an unknowable diversity of biomarkers. With tuneable photophysical properties, synthetic versatility, photostability and a large Stokes shift, the 1,8-naphthalimide has, and continues to be, exploited for the detection of a wide range of enzymatic conversions. This review will outline the recent progress towards the design and synthesis of 1,8-naphthalimide fluorophores for the detection of selected enzymatic conversions.

© 2020 Published by Elsevier B.V.

Contents

1. Introduction

The design and synthesis of small molecules capable of exhibiting fluorescent modulations upon interaction with enzymes and other analytes has received a large amount of research interest in the recent past due to their utility across a broad spectrum of the chemical sciences [1-5]. Such fluorescent sensors provide a number of advantageous characteristics such as facile syntheses, high sensitivity and selectivity, spatiotemporal resolution, and they can be easily tuned to exhibit a diverse range of emission characteristics. Moreover, they provide the basis for the development of sensors for biologically important analytes that can be used as both

* Corresponding author.
E-mail address: robert.elmes@mu.ie (R.B.P. Elmes).
[1] Both authors contributed equally.

https://doi.org/10.1016/j.ccr.2020.213713
0010-8545/© 2020 Published by Elsevier B.V.

diagnostic tools and equally as tools for biologists to better understand the role of those analytes in a given disease state.

Enzyme-Activated probes that seek to operate successfully within the crowded environment of the cell, often encounter additional challenges for the use in biological imaging applications [6] where optimisation of enzyme rates and mode(s) of activation, probe uptake and localisation, probe stability, and cytotoxicity are all important factors. To elicit the desired fluorescent modulations, several techniques have been exploited to date [1,7-11], however, the three most common approaches are outlined in Fig. 1, (**1**) enzymatic cleavage of a blocking group to release an active fluorophore [12-19], (**2**) enzymatic transformation of blocking groups into other substituents [20-24], and (**3**) enzymatic release of a fluorescent quenchers (Fig. 1) [6,25-30]. The full diversity of modulations are discussed in further detail below.

These approaches in turn rely on several photophysical phenomena to induce fluorescence changes. Again, a number of techniques have been exploited to fine-tune fluorescence emission such as Förster Resonance Energy Transfer (FRET), Photoinduced Electron Transfer (PET), Internal-charge Transfer (ICT), Through-bond Energy Transfer (TBET), Excited-state Intramolecular Proton Transfer (ESIPT), Aggregation-induced Emission (AIE), Restriction of Intramolecular Motion (RIM) and Monomer–excimer based ratiometric sensing to name just a few. Many of these topics have been reviewed extensively elsewhere and we will not discuss them in detail here [1,34,35].

Another important consideration in sensor design is the fluorophore scaffold. When designing an optimal fluorogenic substrate, there are various physicochemical characteristics that must be taken into consideration: excitation and emission characteristics [10,36,37], solvatofluorochromism [38], photostability [39], and membrane permeability [40]. As before, several fluorophore options exist for the design and synthesis of responsive probes; rhodamines; coumarins; fluorescein; BODIPYs, cyanines and 1,8-naphthalimides have all been exploited for the detection of a diverse range of enzymatic analytes amongst others [8,9,41,42]. The 1,8-naphthalimide fluorophore in particular has garnered significant attention due to its tuneable photophysical properties and synthetic versatility that provides for a huge diversity of design options [43-46]. The naphthalimide provides two means by which to sense an analyte: by the traditional fluorescence 'switch on' response but equally by tuning the ICT excited state to give a ratiometric fluorescence response. Originally reported by Middleton and co-workers in 1986 [47], the 1,8-naphthalimide core possesses a brightness that is comparable to the coumarins [48], while boasting high resistance to photobleaching and a large Stokes shift. The naphthalimide fluorophore and its inherent photophysical properties are heavily influenced by the electronic character of its substituents. For example, the nitro- functional group – when in the 4-position on the 1,8-naphthalimide core – induces a broad absorption band with λ_{max} at around 360 nm but is largely non-fluorescent. This is due, in part, to the highly electronegative oxy-

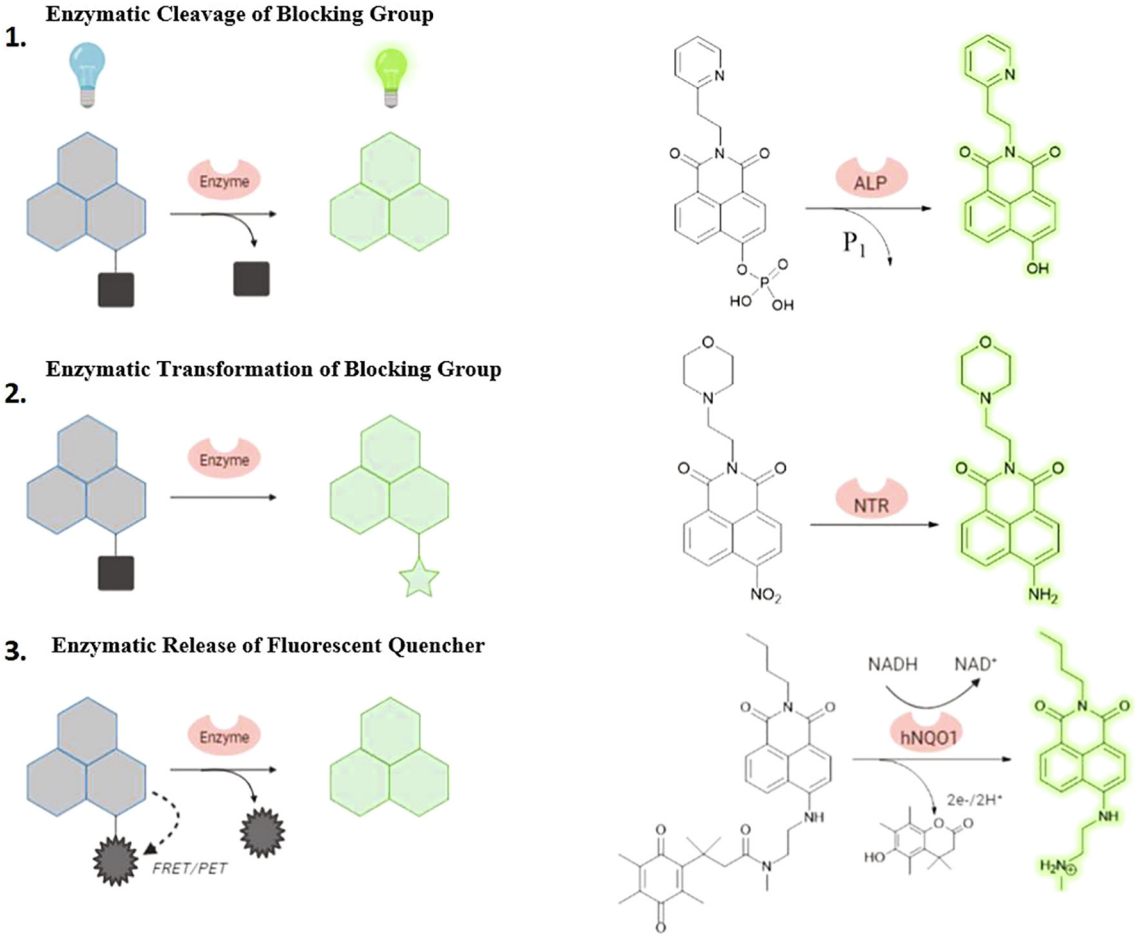

Fig. 1. Schematic representation of scaffolds employed in the design of enzyme-activated 1,8-naphthalimide fluorogenic probes showing specific examples of (**1**) Enzymatic cleavage of a blocking group to release an active fluorophore [31], (**2**) Enzymatic transformation of blocking groups into other substituents [32], (**3**) Enzymatic release of a fluorescent quencher [33].

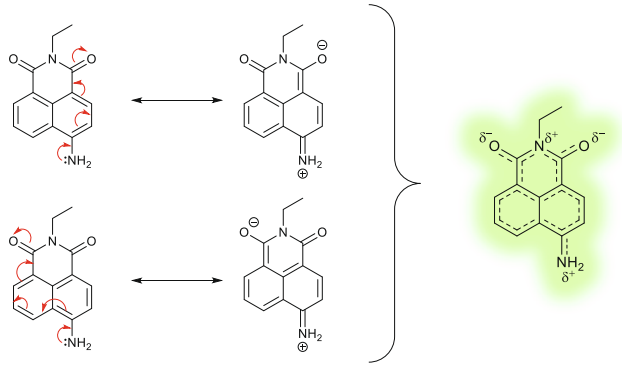

Fig. 2. Schematic of the internal charge transfer within the 4-amino-1,8-naphthalimide fluorophore caused by an electronic "push–pull" system.

gen atoms restricting conjugation of the donor nitrogen to the rest of the fluorophore, effectively blocking ICT. Conversely, the amino-derivative in the same position is "unrestricted" and evokes a "push–pull" ICT excited-state, resulting in broad absorption and emission bands around 450 and 550 nm, respectively (Fig. 2) [43]. Moreover, the amino-nitrogen increases the ICT-character of the fluorophore, resulting in the emission shifting to longer wavelengths when compared with less electron donating substituents such as esters and carbamates. More recently, 4-hydroxy-1,8-naphthalimide has also received significant research attention with absorption maxima in the UV range (*ca.* 380 nm) and corresponding emission maxima at *ca.* 550 nm (or 450 nm in aqueous solutions)[49] with quantum yields in DMSO comparable to those measured for 4-amino-1,8-naphthalimides.

Combined, these properties confer many of the characteristics needed for use in biological applications such as assay design and fluorogenic dyes for confocal microscopy. The ability, to tune the ICT excited-state, in particular, allows for exploitation. For example, installation of an electron-withdrawing carbamate at the 4-position gives rise to 'blue' emission ($\lambda_{max} \approx 450$ nm) being observed and subsequent conversion to the electron-donating amino functional group leads to significant modulation of the optical properties and leads to the observation of green emission ($\lambda_{max} \approx 550$ nm). Ether- and esterification of 4-hydroxy-1,8-naphthalimide also result in a hypsochromic shift of the emission maxima, providing further advantages for the design of fluorescent probes [50,51].

While the 1,8-naphthalimide fluorophore has found success in many areas of research, including: anion recognition [43,52-54], sensing of biologically relevant cations [55], use in OLED research and in the development of novel therapeutics [56] a flurry of interest has recently become apparent in the field of enzyme responsive fluorescent probes. This review will summarise recent progress in the development of 1,8-napthalimide based enzyme sensors and imaging agents where we will attempt to outline key innovations and strategies exploited in the field to date. We will outline various examples that take advantage of a selection of relevant enzyme activators, most of which are directly relevant to new diagnostic and therapeutic applications.

2. Nitroreductases

Nitroreductases (NTRs) are flavin-associated oxidoreductase enzymes (Scheme 1). Classified under two main subgroups; Type I NTRs are capable of reduction in the presence of O_2 while type II NTRs are only active under an oxygen poor environment [57]. Due to the importance of hypoxia in various disease states, type II NTRs have been the focus of intense research in recent years where they are thought to be a valuable biomarker for hypoxic tumour formation. Importantly, they are capable of reducing the nitro functionality to nitroso or amino groups and several NTR based sensors have been reported that take advantage of this fact in both prodrug strategies [58,59] and in fluorometric methods for detection of tumour hypoxia [60,61]. Indeed, given the sensitivity of the "push–pull" ICT excited-state of the 1,8-naphthalimide to changes in its electronic structure naphthalimides are ideally suited to NTR sensing.

Qian and co-workers have developed several fluorescent probes for hypoxia utilising the 1,8-napthalimides (Fig. 3). Conjugating the fluorophore to 2-nitroimidazole gave rise to structures **1** and **2** that, when measured in V79 Chinese hamster, CHO and 95D cells compounds displayed a significant fluorescence response under hypoxic conditions [62], particularly in the case of **2** which displayed 20 times higher emission in cells under hypoxia compared to those under normoxic conditions. Qian and co-workers also took advantage of probes **3** and **4** where **3** was found to display a high degree of fluorescence differentiation between normoxic and hypoxic cells [63]. The same group reported a series of naphthalimide *N*-oxides (**5** – **9**) and showed their DNA binding ability and their application as fluorescent probes for hypoxia [64]. Although, not thought to be targeted by NTR (more likely by cytochrome P450 reductases) these compounds were also capable of differentiating between cells under a hypoxic environment versus those under a normoxic environment. In this report, **5** was shown to be particularly effective, giving a fluorescence response 17 times greater under hypoxic conditions when incubated for 4.5 hrs in V79 Chinese hamster cells. The response was thought to be a result of the *N*-oxide being reduced to the tertiary amine as well as the nitro group being reduced to a primary amine.

An early example of a ratiometric probe for hypoxia using the 1,8-naphthalimdie was demonstrated by Qian and co-workers relying on a *p*-nitrobenzyl moiety conjugated to the 4-amino position through a carbamate linkage to yield compound **10**. This highly selective sensor was 'switched on' by NTR in the presence of NADH and yielded a blue to green fluorescence response due to release of the 4-amino-1,8-naphthalimide fluorophore (a shift in emission from 475 nm → 550 nm) *via* a 1,6 elimination with the simultaneous loss of CO_2 and aza-quinone-methide (Fig. 4). The sensing approach was also capable of detecting hypoxia in A549 cells displaying a similar blue to green response in cells while displaying no cytotoxicity [65].

Ma and co-workers synthesised a naphthalimide based probe **11** that displayed an 'off to on' fluorescence response to NTR. Composed of a morpholine unit conjugated to a 4-nitro-1,8-naphthalimide, **11** was found to be largely non-fluorescent ($\Phi_f = 0.002$ at 543 nm), however, a significant increase in fluorescence ($\Phi_f = 0.13$) was observed upon treatment with NTR caused by the reduction of the $-NO_2$ group to the $-NH_2$ functionality. This resulted in a linear response to NTR concentration and a detection limit of 2.2 ng mL^{-1}. Moreover, the viability of A549 cells was not significantly impacted upon treatment with up to 2 mM of probe. Fluorescence imaging experiments also revealed that the probe could specifically target the lysosomes of living cells (as demonstrated through co-localisation studies with a known commercial lysosomal tracker DND-99) (Fig. 5) and was simultaneously capable of imaging the hypoxic status of A549 cells by imaging the lysosomal NTR activity under hypoxic conditions [32].

He et al. reported the design, synthesis and spectroscopic evaluation of a dual functional ratiometric fluorescent probe, compound **12** that was capable of detecting both nitroreductase and acidity [66]. Taking advantage of a weak intramolecular charge transfer (ICT) in compound **12**, and an efficient photo-induced electron transfer (PET) from the nitrogen atom of a morpholine group to the nitro-group of a 4-nitrobenzyl substituent appended

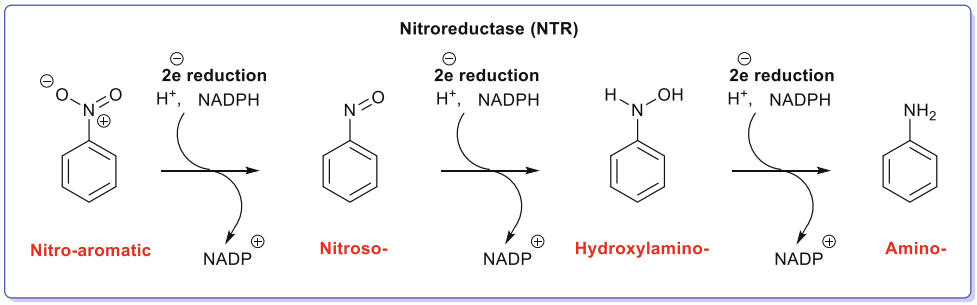

Scheme 1. The reduction of a nitroaromatics in the presence of NTR and NADPH showing the sequential rounds of electron transfers required for complete reduction to the amino group.

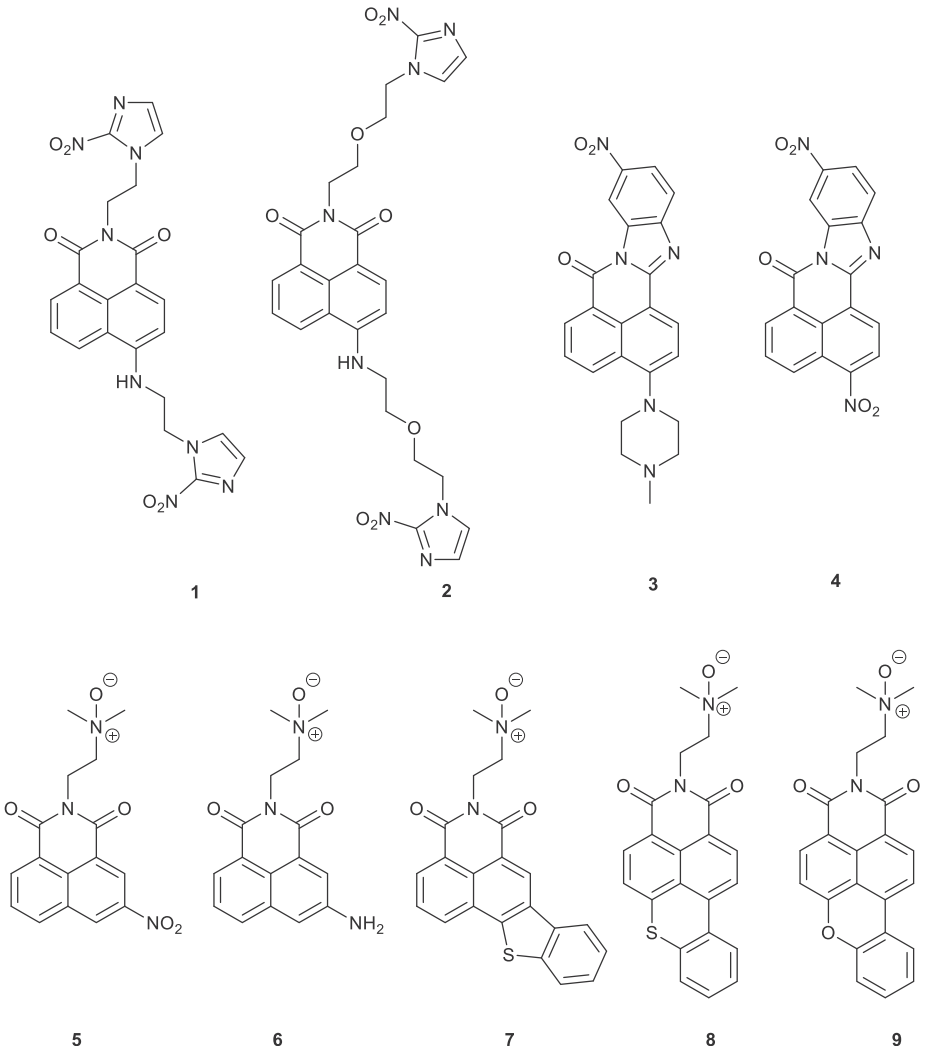

Fig. 3. Chemical structures of compounds **1**–**9**.

to a 1,8-naphthalimide via a carbamate linkage, **12** was shown to be largely quenched in neutral aqueous solution (Φ = 0.02). In an acidic environment, the morpholine group became protonated, thereby 'switching on' weak blue fluorescence (Φ = 0.11) before addition of NTR caused reduction of the 4-nitrobenzyl group that released the highly emissive product **13** (Φ = 0.78). Without both analytical inputs (NTR and acidity) an obvious fluorescence response was not observed. **12** was shown to be highly sensitive (LOD = 0.92 μg mL^{-1} at pH 5) and, using confocal fluorescence microscopy imaging of A549 cells, was also shown to effectively detect acidity and NTR. The authors suggested that compounds of this type may find practical applications in accurate tumour imaging. The sensing process is illustrated in Scheme 2.

In a similar manner, Ma and co-workers have also synthesised a dual functioning probe based on the naphthalimide fluorophore [67]. Taking advantage of a rhodamine/1,8-naphthalimide hybrid structure **14**, containing, nitro- and diethylenetriamine- recognition sites for NTR and ATP, respectively, the authors were able to

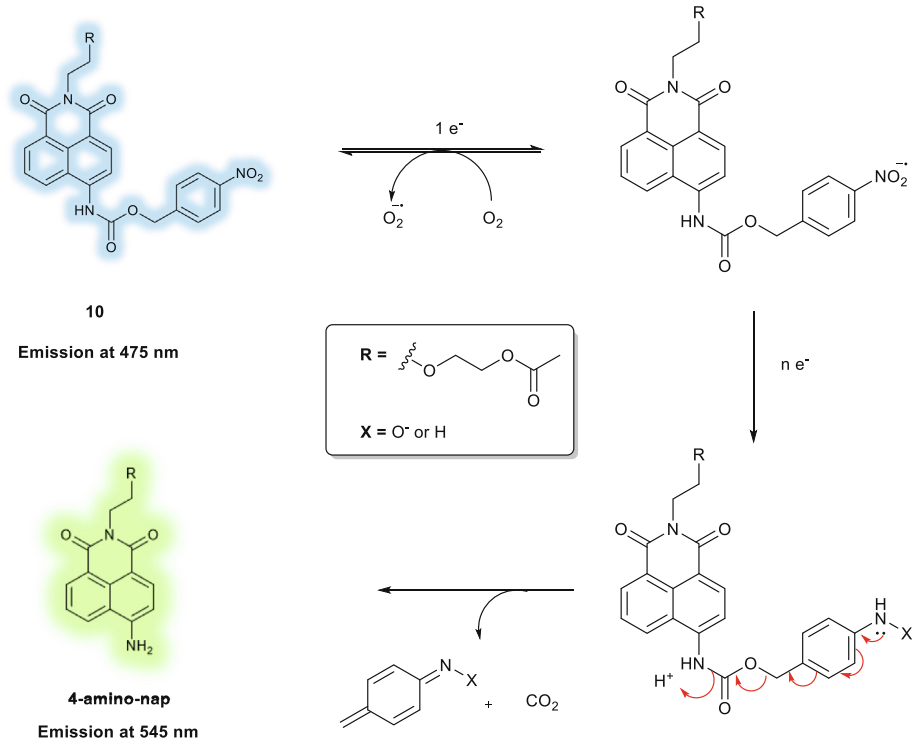

Fig. 4. Proposed detection mechanism of probe **10** based on the 1,6 elimination with loss of CO_2 and aza-quinone-methide.

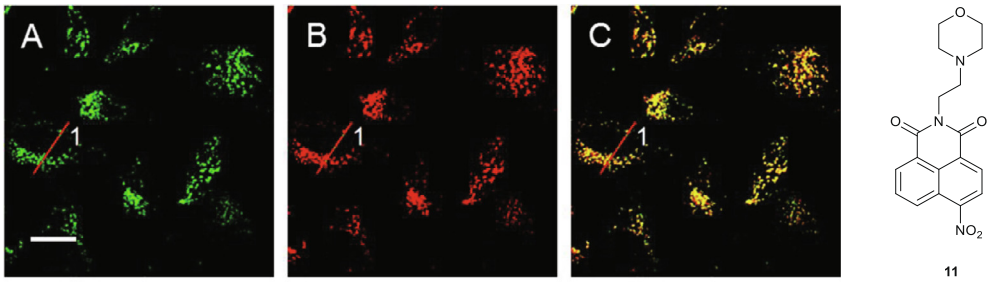

Fig. 5. Colocalization of probe **11** (2 mM) and DND-99 (100 nM) in hypoxic A549 cells. (A) Emission from Lyso-NTR. (B) Emission from DND-99. (C) Merged image of images A and B. Scale bar, 20 mm. Reproduced with permission from *Chem. Asian. J.* **2016**, *11*, 2719–2724.

effectively demonstrate differing fluorometric responses to NTR alone, ATP alone and NTR/ATP combined. **14** exhibited weak fluorescence in its latent state due to quenching effected by the nitro group of the 1,8- naphthalimide and the spirocyclic rhodamine structure. Addition of NTR resulted in an increase in emission at 520 nm resulting from nitro reduction leading to formation of the highly emissive 4-amino-1,8-naphthalimide moiety (verified by ESI-MS analysis). Similarly, addition of ATP also resulted in an increase in fluorescence, this time at 580 nm, attributed to the ring-opening of the spirocyclic structure of rhodamine in the presence of ATP. A linear relationship between change in fluorescence and analyte concentration was observed in both cases resulting in LODs of 0.12 μg/mL and 0.05 mM for NTR and ATP, respectively. Given the independent emission wavelengths of both fluorophores, the authors also demonstrated the ability of **14** to detect NTR and ATP concentrations simultaneously in the same solution by adjusting the excitation wavelength. Application of this probe was shown through confocal fluorescence microscopy where, again, it was possible to address the probe through varying excitation wavelengths to determine the presence of both NTR and ATP. Interestingly, this probe was applied to HeLa cells, and suggests that ATP levels in cells are significantly affected depending on the O_2 concentration. Indeed, the experimental results revealed that decreasing the O_2 content from 20% to 1% resulted in an increase in the activity of intracellular NTR with a concomitant decrease in the intracellular ATP concentration (Fig. 6).

The utility of napthalimide based probes for NTR has also recently been demonstrated by Zhang et al. who have reported the use of **15** for NTR in both bacterial and mammalian cells (Fig. 7) [68]. Composed of a 4-hydroxy-1,8-naphthalimide conjugated to a 4-nitrobenzyl moiety, **15** displayed a 'switch on' fluorescence response (λ_{em} = 489 nm) to NTR in the presence of NADH (LOD = (3.4 ng mL^{-1}) and the authors were able to show using confocal microscopy that the probe was able to enter *E.coli* and *S.aureus* cells whereby blue emission was seen to increase in intensity upon reaction with intracellular NTR. Similarly, treatment of HepG-2 and MCF-7 cancer cells resulted in a dose-dependent increase in fluorescence while remaing non-toxic to those cells. A related probe **16**, this time exploiting a carbonate linker, was reported by Wei et al. who demonstrated that **16** exhibited a strong increase in green fluorescence at 550 nm after reaction with NTR and NADH [69]. Again, the fluorescence of this probe increased linearly over the range of 0.1–0.3 mg mL^{-1} NTR and was exploited to image U87 cells under hypoxic conditions.

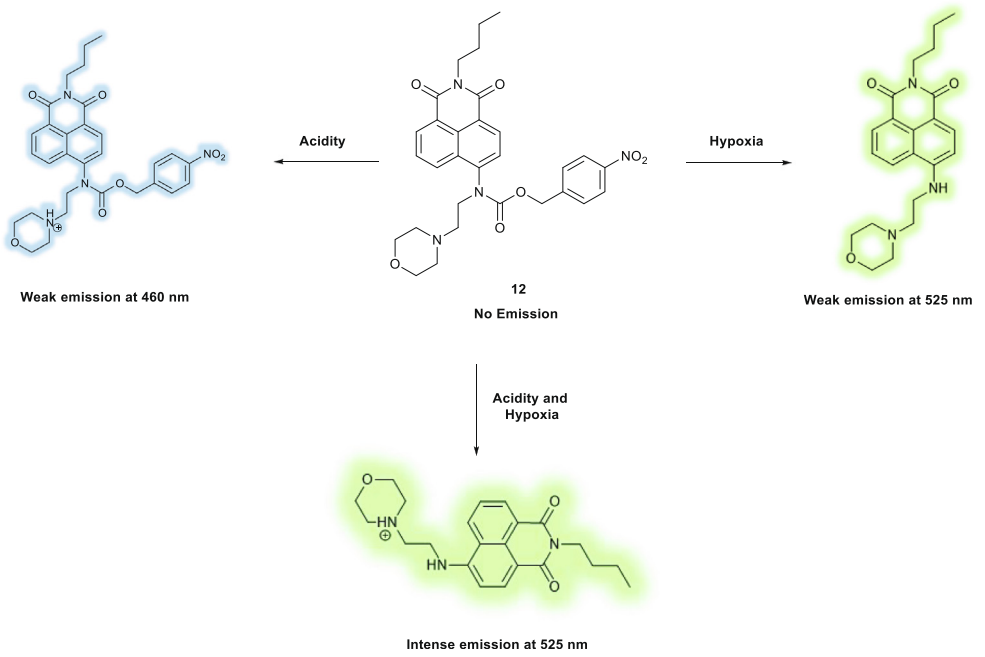

Scheme 2. Proposed detection mechanism of probe **12**.

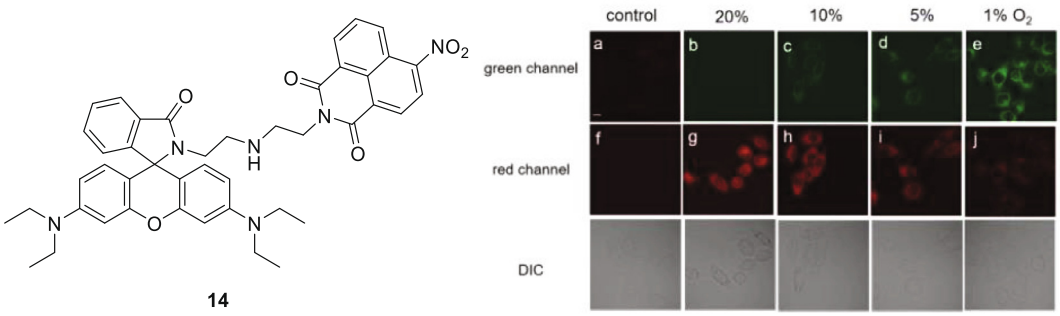

Fig. 6. Chemical structure of probe **14** and confocal fluorescence images of HeLa cells treated with probe **14** under varying O_2 concentrations (20%, 10%, 5% and 1%). Green (λ_{ex} = 405 nm, λ_{em} = 430–530 nm) and red (λ_{ex} = 559 nm, λ_{em} = 570–670 nm) channels were detected, independently. Reproduced with permission from *Chem. Commun.* **2018**, *54*, 5454–5457.

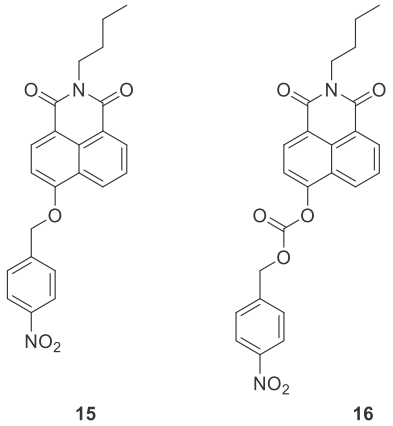

Fig. 7. The chemical structures of probes **15** and **16**.

Xu et al. reported a 4-nitro-1,8-naphthalimide probe **17** containing a methylsulphonamide moiety capable of directing the probe to the endoplasmic reticulum (Fig. 8) [70]. **17** took advantage of the ability of NTR to reduce the 4-nitro functionality to the 4-amino derivative thereby resulting in a 'switch on' of the naphthalimide internal charge transfer (ICT). The result was a sensitive (LOD = 36 ng mL^{-1}), selective and biocompatible probe that had the added benefit of being compatible with both one-photon and two-photon excitation due to it's high degree of photostability. The authors demonstrated it's ability to image NTR in HeLa cells whereby cells displayed no fluorescent signal under normoxic conditions (21% O_2) but under hypoxic conditions (15–1% O_2) significant fluorescence was observed (Fig. 6). Moreover, co-localisation studies conducted with ER-Tracker Red showed a high degree of co-localisation (Pearson's colocalisation coefficient = 0.90), and the spatial distribution of both signal appeared to be consistent with each other. **17** was finally applied to mouse tumour tissues where two-photon fluorescence excitation was also applied to successfully image the activity of endogenous NTR in these tissues.

Our research group, has taken advantage of the the synthesis of two 2-nitroimidazole-1,8-naphthalimide conjugates **18** and **19** [20]. As with previous examples, these probes exploit a reduction–fragmentation mechanism, to yield a ratiometric fluorescent response to NTR that be clearly seen with the naked eye (Fig. 9).

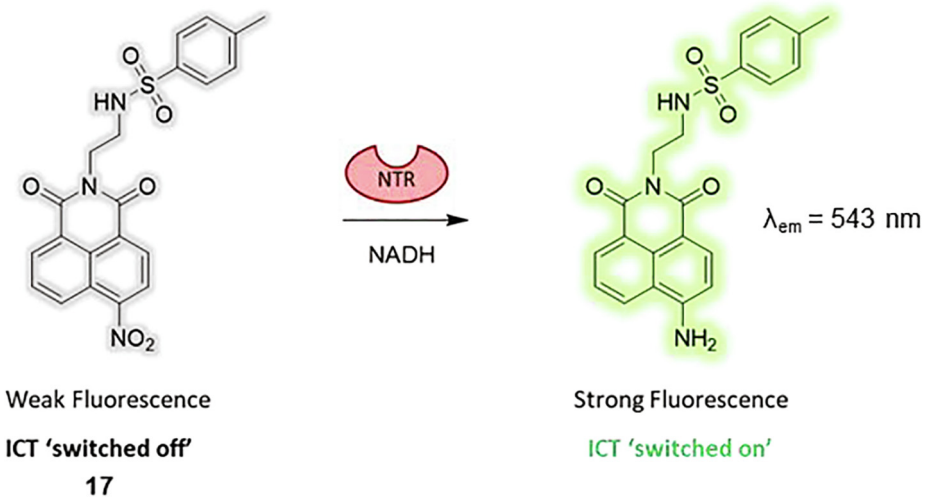

Fig. 8. The chemical structure of probe **17** and and a schematic representation of the proposed mechanism of NTR recognition.

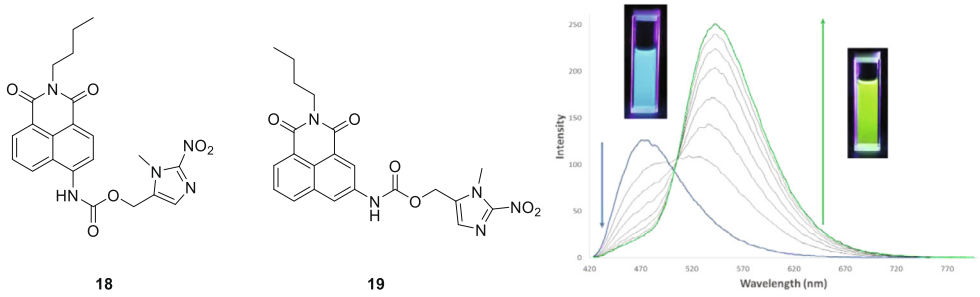

Fig. 9. The chemical structures of **18** and **19** and the fluorescence changes seen for **18** (10 μM) (λ_{ex} = 345 nm) over 10 min after adding NTR (1 μg mL^{-1}) (Inset): Naked eye changes seen under UV irradiation.

Importantly, the 2-nitroimidazole appears to be significantly more sensitive to NTR compared to it's 4-nitrobenzyl analogue and a linear response was observed over a concentration range of 0.02–5 μg mL^{-1} NTR. Indeed, **18** was shown to successfully detect reductive stress in HeLa cells using both confocal microscopy and flow cytometry while being effectively non-toxic to cells.

Jolliffe, New and co-workers have reported a series of hypoxia-responsive 1,8-naphthalimides for biological imaging applications and several methods to synthesise a more diverse pool of available structures [71,72]. While most known 1,8-naphthalimides are functionalised either at the imide and 3 or 4-positions some recent work provided a means to also incorporate substitution at the 6-position. This approach provides increased versatility to the fluorophore scaffold allowing the synthesis of molecules that contain a sensing group, a targeting group and an ICT donor to optimise photophysical characteristics. Indeed, using their approach that relied first on the synthesis of key intermediate **20** and through functionalisation at the imide position with aspartic acid and a subsequent Suzuki coupling, the authors synthesised **22** as a hypoxia sensor successfully imaging the hypoxic and necrotic regions of DLD-1 tumour cell spheroids (Fig. 10) [73].

Another recent piece of work by Tang and co-workers reports a ratiometric fluorescent probe based on a water-soluble conjugated polymer functionalised with a *p*-nitrobenzene modified 1,8-naphthalimide **23** (Fig. 11). The fluorescence of this material is quenched by both FRET between the polymer and the naphthalimide, and a photoinduced electron transfer between the naphthalimide and nitrobenzene group, resulting in a very low background signal. However, upon reduction of the NO_2 group by NTR, FRET is 'switched on' and the PET is blocked resulting in a large fluorescence increase at 526 nm yielding a detection limit of 19.7 ng/mL. This material exhibited good selectivity and low cytotoxicity, and

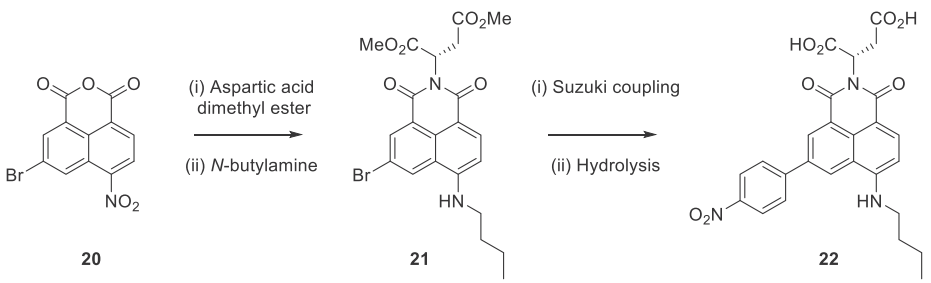

Fig. 10. The chemical synthesis of **22** through intermediates **20** and **21** and confocal microscopy images of DLD-1 spheroids treated with **22** (scale bar represents 100 mm). Reproduced with permission from *Chem. Eur. J.* **2020**, 26, 10,064 –10071.

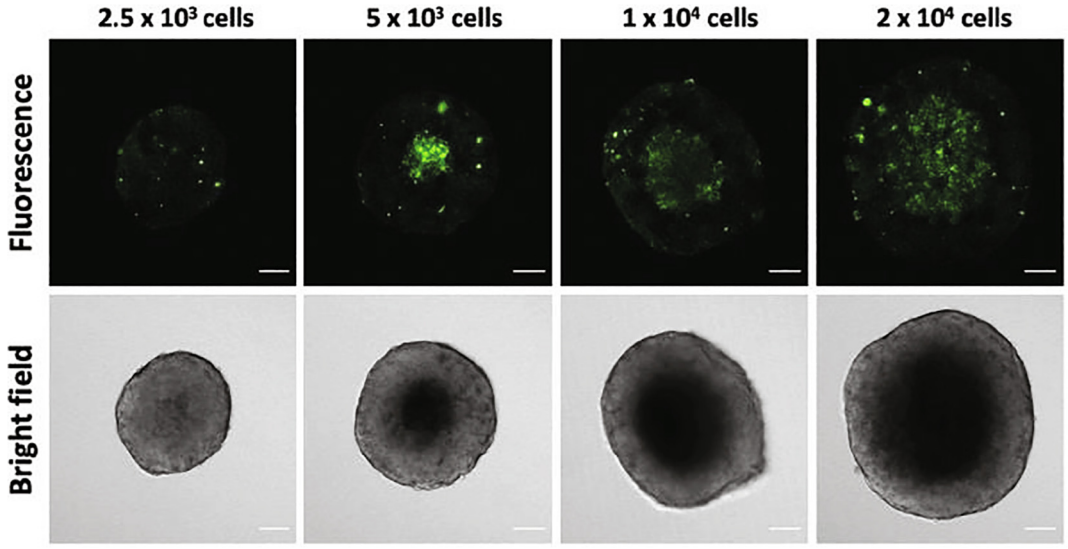

Fig. 10 (*continued*)

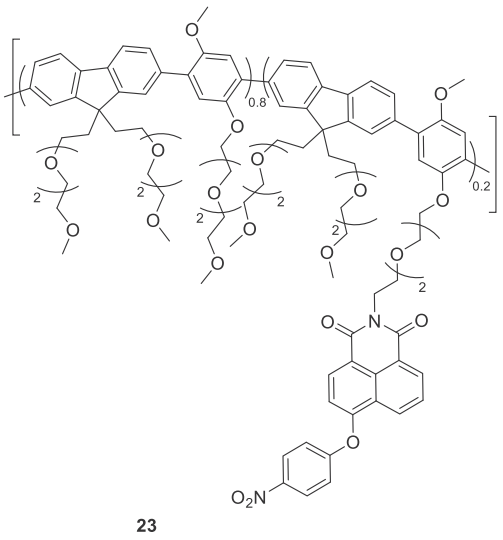

23

Fig. 11. The chemical structure of conjugated polymer **23**.

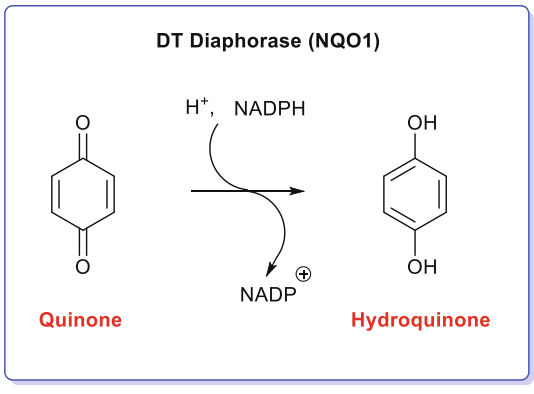

Scheme 3. The two-electron reduction of a quinone to a hydroquinone in the presence of NQO1 and NADPH.

was also demonstrated to be useful to image intracellular detection of NTR in hypoxic A549 tumour cells [74].

3. DT-diaphorase

NAD(P)H:quinone oxidoreductase 1 (NQO1) also known as DT-diaphorase is a well-known cytosolic flavoenzyme [75]. NQO1 is most notably involved in the 2-electron reduction of quinones to their corresponding hydroquinones in the presence of an electron donor NADH or NADPH (Scheme 3) [76,77]. Although NQO1 is an established antioxidant, more interestingly it is a stabilizer of tumour suppressors (e.g., p53, p73α, and p33) preventing their degradation by the 20S proteasome [78]. Furthermore, a significant upregulation of NQO1 is associated with a variety of cancers e.g., non-small cell lung carcinoma, colorectal carcinoma, and ovarian carcinoma [79,80]. Several naphthalimide based fluorescent probes have taking advantage of the photo-induced electron transfer (PET) quenching mechanism [81,82].

McCarley and co-workers have developed both sensitive and selective turn on fluorescent probes for cancer associated enzyme human NAD(P)H: quinone oxidoreductase isozyme 1 (hNQO1) (Fig. 15). Structure **24** consists of a quinone substrate capable of quenching *N*-methylethanolamine linked 4-amino-*N*-butyl-1,8-naphthalimide by oxidative electron transfer. Upon two electron reduction of the quinone substrate, in the presence of NQO1, the naphthalimide moiety is released as a result of lactonization (Scheme 4). Possessing a higher rate of activation in the presence of hNQO1 amongst other probes based on NQO1 activation, **24** was shown to be both selective and sensitive for hNQO1 *in cellulo*. Flow cytometry assays (λ_{ex} = 405 nm, λ_{em} = 457/60 nm) showed that colorectal carcinoma cell line HT-29 and the non-small cell lung cancer A549 (hNQO1 positive cell lines) displayed high intensity signals when incubated with **24**, with no change in intensity when comparing incubation periods of 60 and 10 min. Moreover, much lower fluorescence intensities were observed for hNQO1 negative cell lines H596 and H446. Confocal microscopy studies showed a cytosolic blue fluorescence signal increase by 9-fold in A549 cells and 23-fold in HT-29 cells in comparison to H596 cells (Fig. 12). Two photon confocal microscopy (λ_{ex} = 750 nm) also displayed significant fluorescence increases in A549 and HT-29 cells with 13 and 15-fold increases respectively compared to H596 cells [33].

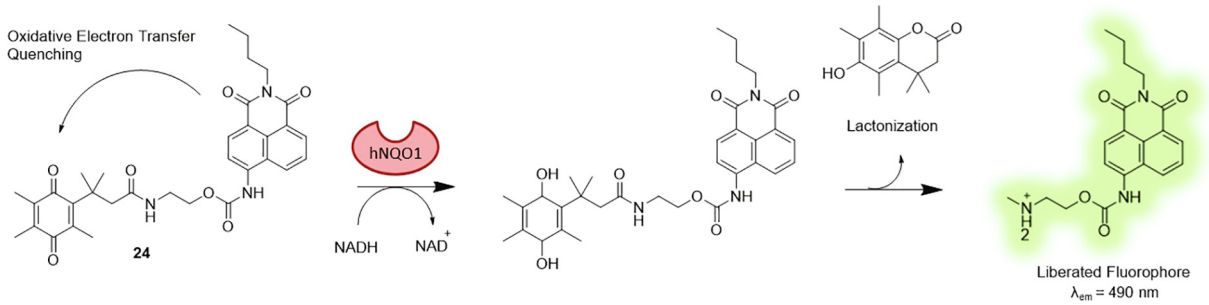

Scheme 4. Schematic showing reduction of quinone substrate of Probe **24** to liberated naphthalimide fluorophore.

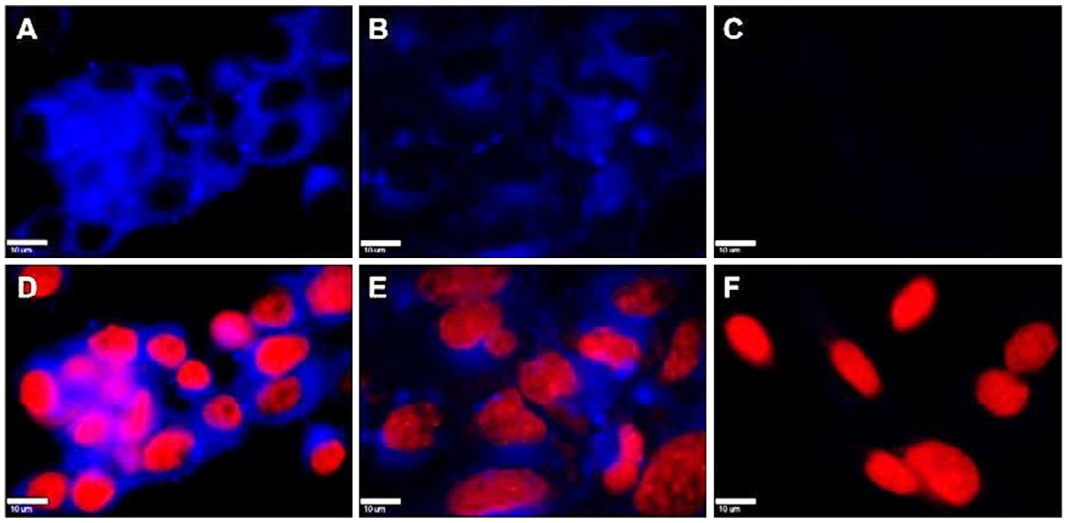

Fig. 12. Wide field microscopy images of HT-29 cells (A and D), A549 cells (B and E), and H596 cells (C and F). The top row consisting of images of the released naphthalimide fluorophore. The bottom row overlaying the fluorescence of the naphthalimide with cell nuclei labelled with red dye. Images taken after a 10-minute incubation period with **24**. Reproduced with permission from *J. Am. Chem. Soc.*, **2013**. 135, 309–314. Copyright 2013 American Chemical Society.

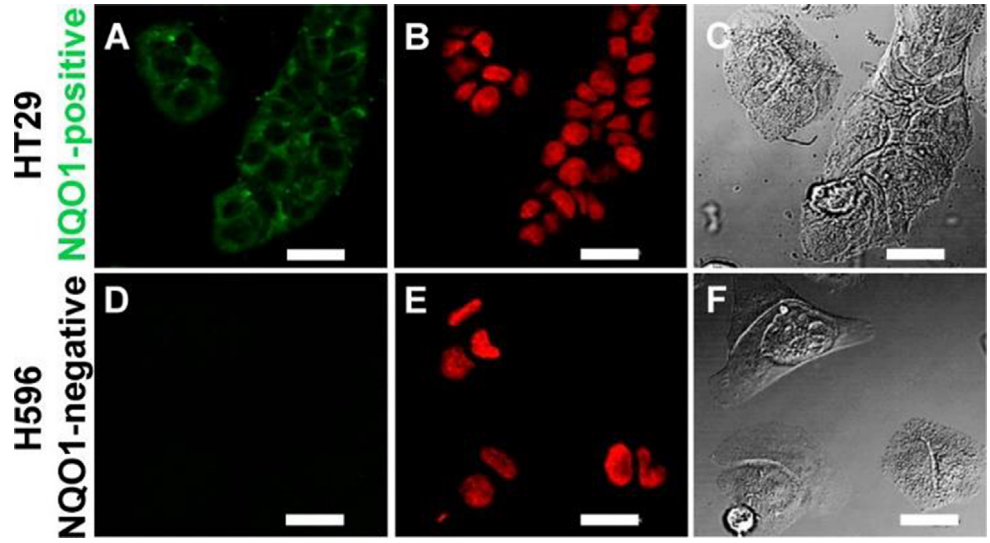

Fig. 13. Confocal microscopy images displaying fluorescence output (A) of **25** in hNQO1 positive HT29 cells in comparison to no fluorescence observed in H596 hNQO1 negative cell line. Nuclear stain (DRAQ5) used in images (B, E). Differential contrast images provided in images (C, F). Reproduced from *J. Am. Chem. Soc.*, **2014**, 7575–7578. Copyright 2014 American Chemical Society. https://pubs.acs.org/doi/10.1021/ja5030707, further permissions related to the material excerpted should be directed to the ACS.

Like **24**, compound **25** made use of the same quinone substrate and naphthalimide reporter but differed by the incorporation of a self-immolative linker moiety. By taking advantage of PET and the use of an *N*-methyl-*p*-aminobenzyl alcohol self-immolative

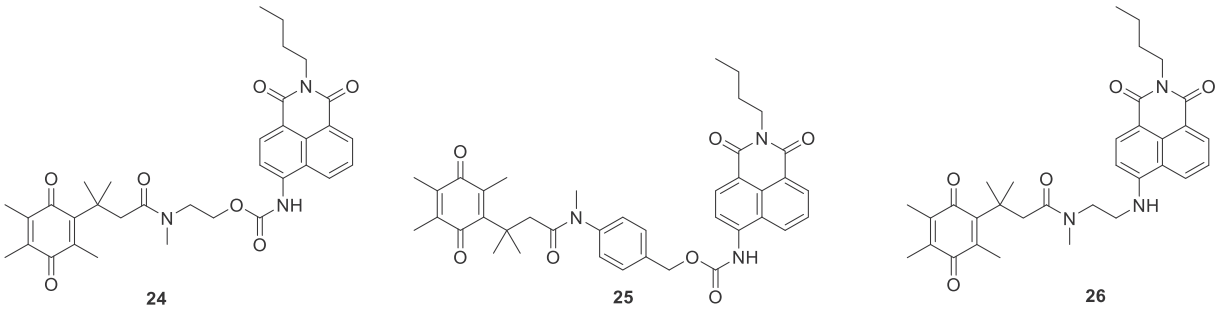

Fig. 14. The chemical structure of compounds **24**–**26**.

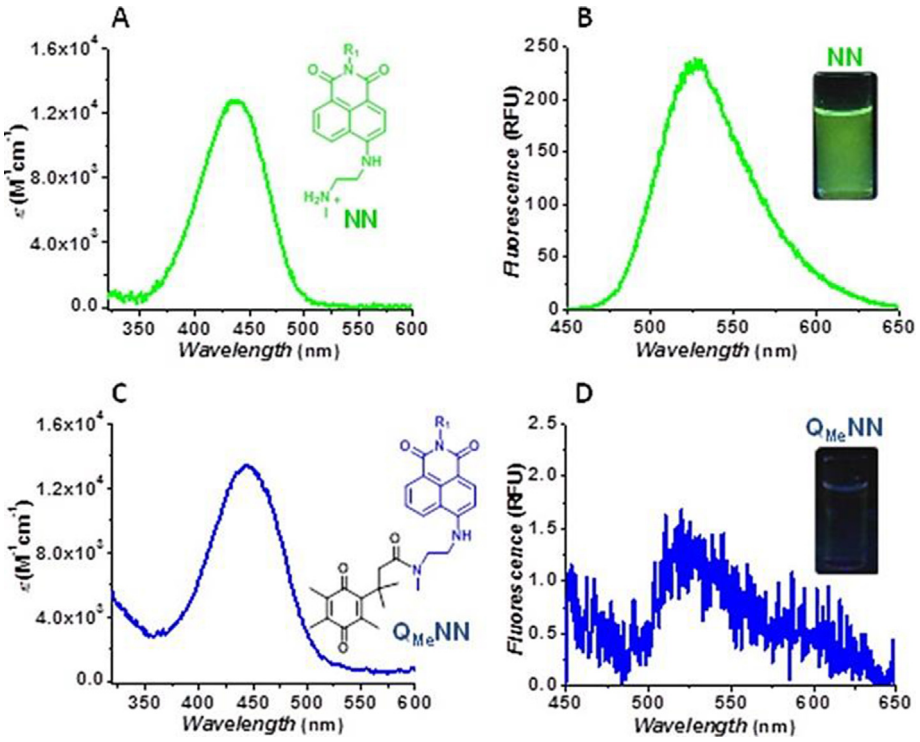

Fig. 15. The absorption (C) and emission (D) of **26** and the absorption (A) and emission (B) of the naphthalimide reporter. R substituted with n-butyl. Fluorescence emission spectra excited at 440 nm. Reproduce from *Anal. Chem.* **2015**, 6411–6418. Copyright 2015 American Chemical Society.

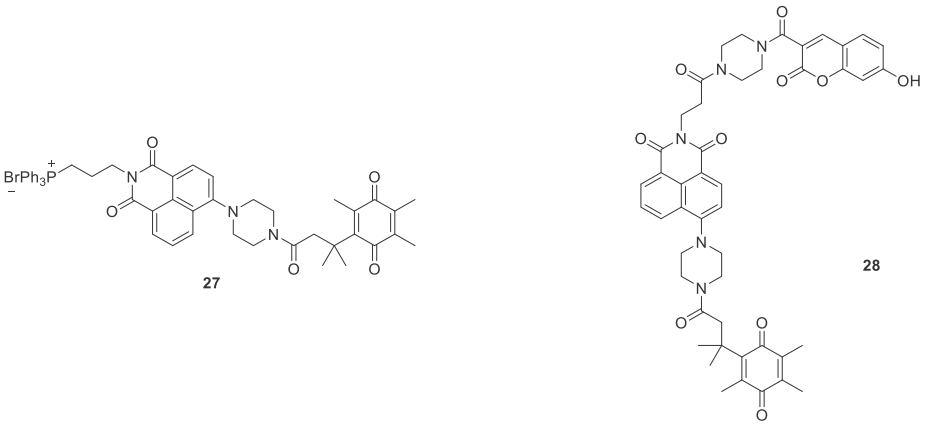

Fig. 16. Compounds **27** and **28**.

linker, a fluorescent enhancement at 532 nm was achieved by the naphthalimide reporter unit. *In vitro* studies established the formation of the naphthalimide reporter with increases in fluorescence at an exceptional rate upon incubation of the probe in the presence

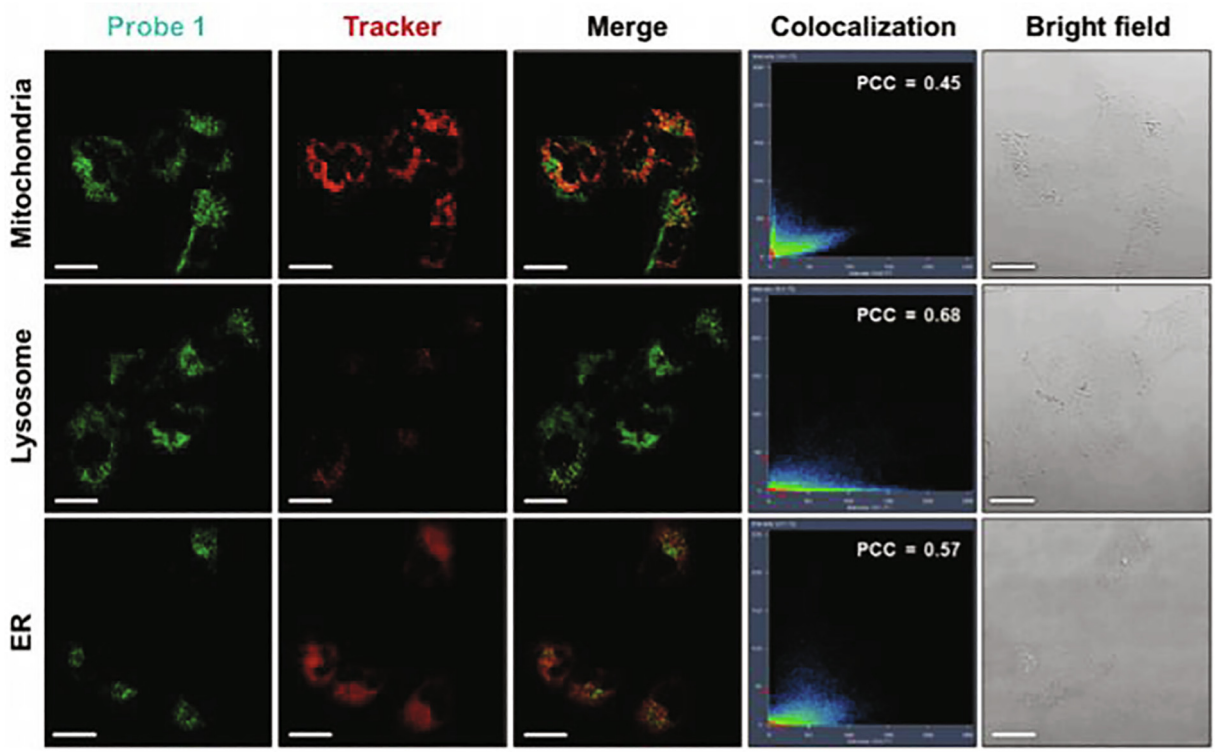

Fig. 17. Confocal microscopy images showing the colocalization of probe **27** and sub-organelles in A549 cells following an incubation period 1 h at 37 °C with 5 μM of **27**. Sub-organelles (mitochondria, Lysosome, Endoplasmic reticulum) were stained with relevant trackers. The PCC values seen under colocalization is an indicator Pearson's correlation coefficient. Reproduced with permission from *MDPI. Sensors* **2020**, *20*, 53.

of hNQO1 and NADH under physiological conditions *via* lactonization followed by rapid self-immolative cleavage of the *N*-methyl-*p*-aminobenzyl alcohol. Confocal fluorescence microscopy imaging displayed uptake and activation of **25** was observed by green fluorescence in HT29 colorectal cancer cells (hNQO1 positive) with minimal fluorescence observed in H596 lung cancer cells (hNQO1 negative) (Fig. 13). The 95-fold fluorescent increase observed demonstrates the stability of **25** and the fluorescence efficiency of the naphthalimide reporter [83].

In a related study, it was shown that Probe **26**, with a less bulky and shorter linking unit, displayed enhanced photophysical properties. Fluorescence quantum yields of the naphthalimide reporter versus **26** differed by 120-fold (Fig. 14). Evaluation of hNQO1 to activate **26** showed that the less bulky linker is responsible for the higher catalytic efficiency in comparison to previously synthesised **24** by 100-fold. Furthermore, uptake and activation of **26** was observed through obvious green fluorescence in both colorectal HT-29 cells and ovarian cancer cell line (NIH: OVACAR-3). High sensitivity and selectivity coupled with low toxicity, renders **26** applicable for *in vivo* imaging studies as a hNQO1 turn on fluorescent probe [33,84].

Min Hee Lee *et al.* also reported the synthesis of naphthalimide based fluorescent probes consisting of a quinone substrate (Fig. 16). By introducing a triphenyl phosphonium salt onto the naphthalimide moiety of probe **27** rapid detection of hNQO1 was achieved under physiological conditions. Significant fluorescence intensity increases were also observed for the triphenyl phosphonium naphthalimide piperazine **27** at 540 nm in comparison to n-butyl naphthalimide piperazine. Confocal microscopy demonstrated the uptake of **27** in A549 cells with clear green fluorescence while only weak fluorescence was observed in H596 cells. Moreover, with the use of organelle-selective staining dyes it was revealed that **27** was localised to the endoplasmic reticulum, lysosomes, and mitochondria in A549 cells (Fig. 17). Selectivity of the probe in A549 cells was also evidenced by the pre-treatment of cells with dicoumarol, an hNQO1 inhibitor, as seen by a notable decrease in fluorescence intensity upon treatment. Probe **28** based on dual emission of a coumarin-naphthalimide hybrid was also reported where it was shown to take advantage of trimethyl locked quinone propionic acid as an hNQO1 enzyme substrate (Scheme 5). Activity of hNQO1 could be monitored *via* the changes at two emission wavelengths (emission at 460 nm and 540 nm) upon reduction and cyclisation of the quinone moiety, with saturation of fluorescence response within 30 min. The fluorescence intensity ratio (I_{540nm}/I_{460nm}) was analysed and showed a significant increase upon 2-hours of incubation with A549 cells while in the presence of A549 cells pre-treated with dicoumarol the response was significantly less (Fig. 18). **28** shows potential to be used for *in vivo* imaging of hNQO1 as a result of its ratiometric fluorescence response in A549 cells [85,86].

4. Other oxidoreductases

Other members of the Oxidoreductase family, such as Thioredoxin reductases (TrxRs) are responsible for vital functions *in vivo*, carrying out various roles towards the maintenance of intracellular redox homeostasis through a two-electron reduction of disulfides to thiols in the presence of NADPH (Scheme 6). TrxRs such as TrxR1 and TrxR2 are structurally similar, where they share the same highly reactive C-terminus selenocysteine residue that possesses a wide substrate margin. This results in both TrxRs being involved in similar roles such as DNA repair and gene transcription [87-91]. Moreover, in many diseases such as cancer and neurodegenerative diseases, TrxRs may be overexpressed or malfunction and are thus represent an interesting target for fluorescent probes [92,93].

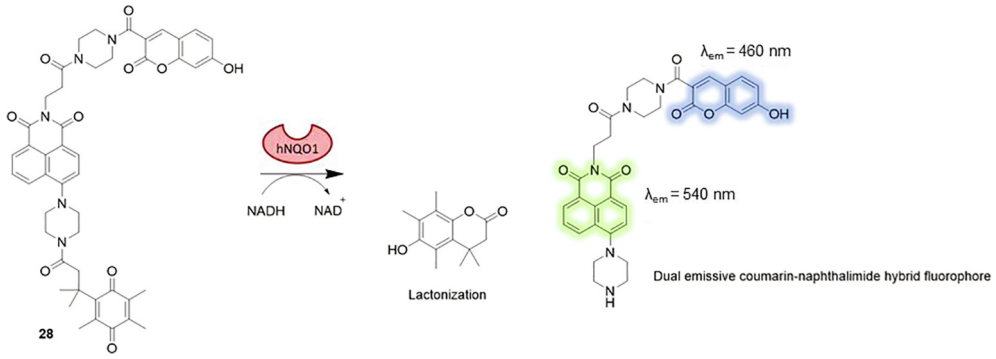

Scheme 5. Schematic showing reduction of quinone substrate of Probe **28** to liberated dual emissive naphthalimide/coumarin hybrid fluorophore.

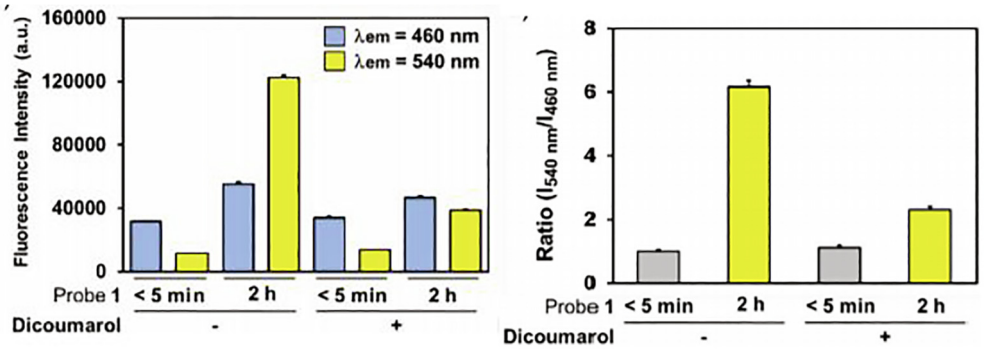

Fig. 18. (Left) Inhibitory assay of NQO1 activity measured with Probe **28**, using dicoumarol as an inhibitor. A549 cells were treated with **28** (10 μM). (Right) Shows the Fluorescence intensity-ratio of **28**. Reprinted from *Dyes and Pigments*, Volume 164, Park, S. Y.; Won, M.; Kang, C.; Kim, J. S.; Lee, M. H. A coumarin-naphthalimide hybrid as a dual emissive fluorescent probe for hNQO1, Pages 341–345, Copyright 2019, with permission from Elsevier.

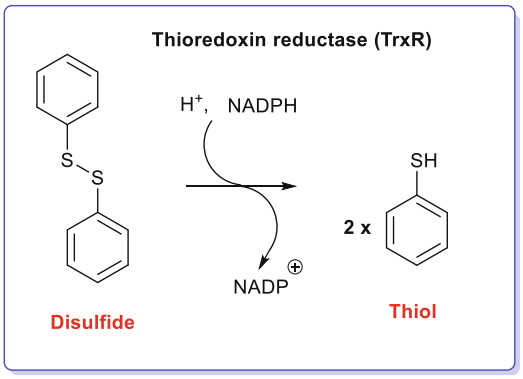

Scheme 6. The two-electron reduction of a disulfide to a thiol in the presence of TrxR and NADPH.

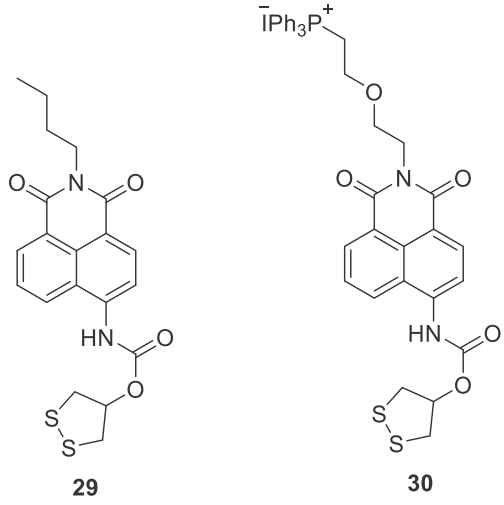

Fig. 19. Probes **29** and **30**.

Fang and co-workers developed fluorescent probe **29** (Fig. 19) for thioredoxin reductase (TrxR), featuring a 4-amino-*n*-butyl-1,8-Naphthalimide moiety and a 1,2-dithiolane enzyme substrate acting to quench the naphthalimide fluorescence. Under physiological conditions, reduction of **29** by TrxR and NADPH *via* disulphide bond cleavage yields a five membered cyclic carbamate and free naphthalimide caused by an intramolecular cyclisation; a fluorescence enhancement observed at 538 nm results. **29** was also shown to be highly selective amongst intracellular thiols and reducing agents. Interestingly, U498C, a mutant enzyme of TrxR, shows just a minor increase in fluorescence intensity even at elevated concentrations, establishing the significance of the selenocysteine residue unique to TrxRs involved in the reduction mechanism. Moreover, **29** was capable of imaging TrxR in live Hep G2 cells with bright green fluorescence observed after an incubation period of just 4 h. Notably, a significant decrease in fluorescence was observed when Hep G2 cells were previously treated with 2,4-dinitrochlorobenzene (DNCB); a TrxR inhibitor (Fig. 20) [94].

Fang *et al.* also reported a selective turn on fluorescent probe **30** (Fig. 19) for imaging thioredoxin reductase 2 (TrxR2). The probe was analogous to **29** but differed due to the incorporation of a triphenyl phosphonium group at the imide position of the naphthalimide. This structural change improved the hydrophilicity of

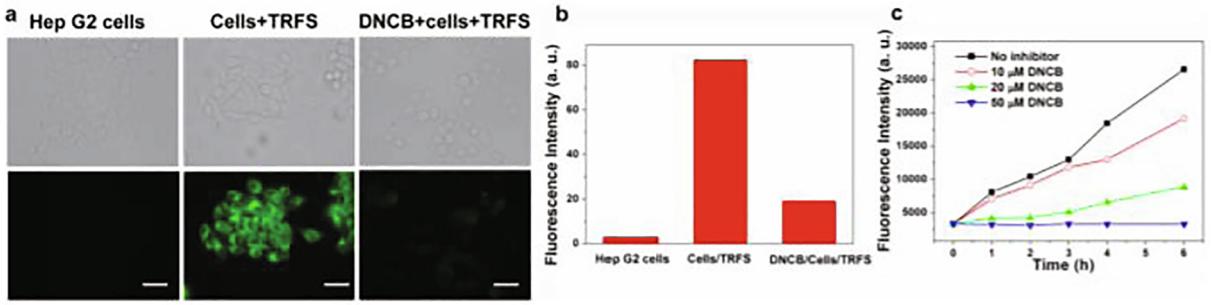

Fig. 20. (a) Probe **29** Fluorescence in Hep G2 cells. (b) Relative Fluorescence intensity in a single cell. (c) Quantification of fluorescence in Hep G2 cells following treatment with varying concentrations of DNCB. Reprinted with permission from *J. Am. Chem. Soc.* 2014, 136, 1, 226–233. Copyright 2014 American Chemical Society.

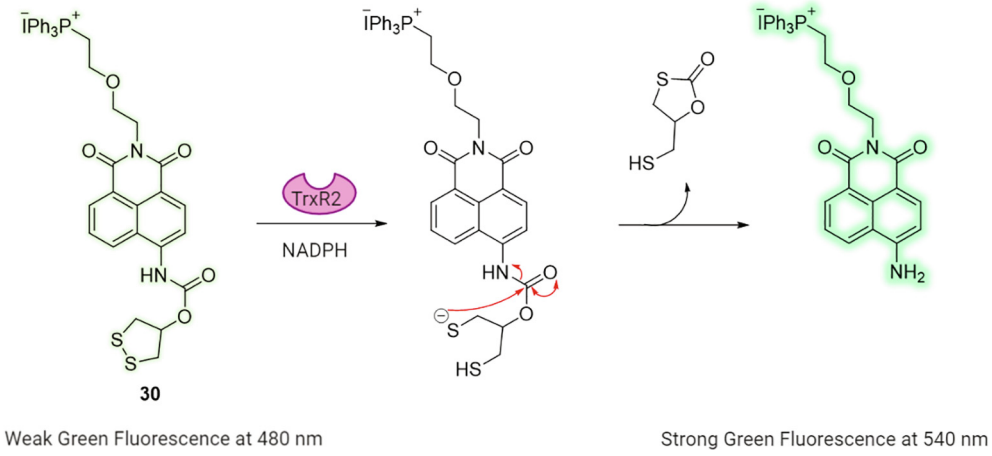

Scheme 7. Schematic of TrxR2 acting upon **30**.

30 and aiding electrostatic interaction with the negatively charged C-terminus of the TrxR active site. This change also resulted in a 30-fold increase in fluorescence intensity response to TrxR at 540 nm within 60 min (Scheme 7). **30** exhibited high selectivity for TrxR in HeLa cells visualised as an increase in green fluorescence. Fluorescence colocalization studies also revealed that **30** was confined to the mitochondria as a consequence of the triphenyl phosphonium moiety. Furthermore, flow cytometry showed a significant decrease in relative fluorescence intensity of **30** in a Parkinson's disease cell model in which the activity of TrxR2 is suppressed;[93] this renders **30** as a useful biomarker for Parkinson's disease.

5. Oxidases

As a sub-class of oxidoreductases, oxidases are classified by the specificities of their redox reaction and what is the terminal electron acceptor – in the case of oxidases molecular oxygen (O_2) is the terminal acceptor. In contrast, dehydrogenase(s) remove hydrogen atoms from a donor in an NAD^+- or FAD-conditional procedure [6]. Probes **31** & **32** (Fig. 21) – reported by the groups of Singh and Ma, respectively – were designed for the recognition of tyrosinase, an oxidase capable of oxidation of a hydroxyaromatic to a catechol and ultimately a quinone in the presence of O_2 (Scheme 8) [95,96]. Inequality in tyrosinase activity has been correlated with different diseases – some being neurodegenerative – such as dopamine neurotoxicity, schizophrenia, and Parkinson's disease. Likewise, upregulation of tyrosinase can be interconnected to the formation of melanomas [97]. Because of this, tyrosinase activity can act as an effective indicator for the clinical diagnosis

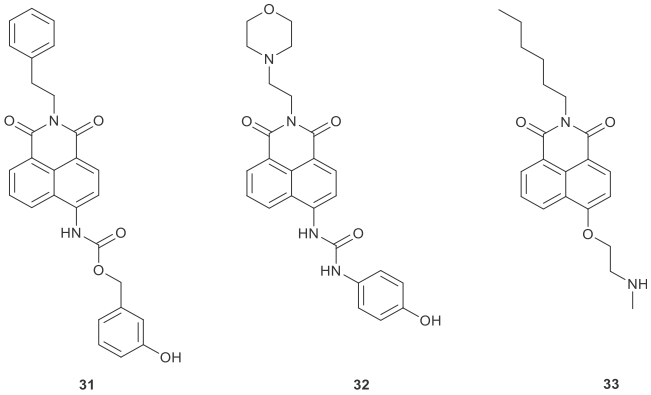

Fig. 21. Chemical structures of compounds **31**–**33**.

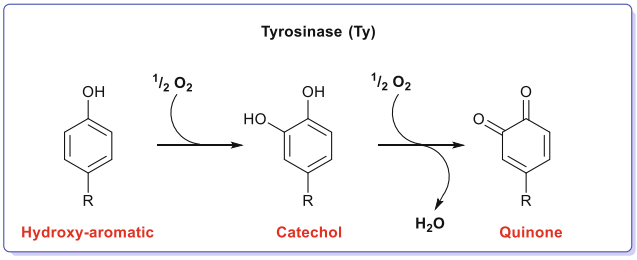

Scheme 8. The oxidation of a hydroxyaromatic to a catechol and ultimately a quinone in the presence of O_2 and Ty.

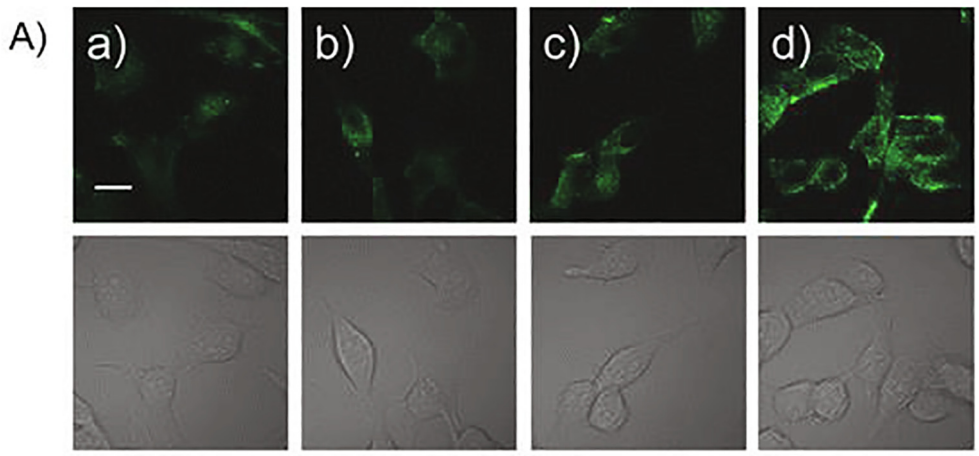

Fig. 22. Confocal fluorescence images (a) B-16 cells were incubated with Probe **32**; (b) Pre-treated with 8MOP for 12.0 hrs and then addition of Probe **32**; (c) Exposed to UV-A then addition of Probe **32**; (d) Pre-treated with 8MOP for 12.0 hrs, then exposed to UV-A then addition of Probe **32**. Reprinted from *Anal. Chem.* **2016**, 88, 8, 4557–4564, *Copyright © 2016, American Chemical Society.*

of tumour cells and uneven pigmentation of skin cells. 3-Hydroxyphenyl – an important feature in the design of probe **31** – was covalently coupled to 4-amino-1,8-naphthalimide via a carbamate linkage, which mitigates interference of free radicals and other biologically-relevant analytes.

The change in the fluorescence emission colour of probe **31**, from blue (467 nm) to green (535 nm) with incremental additions of tyrosinase to the reaction mixture was observed. As the reaction progressed, the emission at 535 nm increased regularly with elevated amounts of tyrosinase being added. In short, a ratiometric change in fluorescence was observed. **31** also demonstrated significant selectivity and sensitivity to the enzyme, with a detection limit of 0.2 U mL^{-1}. Ma and co-workers took a slightly different approach with the design of probe **32**, incorporating a 1,8-naphthalimide with a morpholine and 4-aminophenol-modified urea trigger. In contrast to probe **31**, **32** exhibits an 'off-on' feedback response to tyrosinase *via* an oxidation-type cleavage reaction. Curiously, the probe was observed to fluoresce in melanosomes, although it was shown to partially localise in other acidic regions such as lysosomes. By utilising and expanding on this property of **32**, Ma *et al.* imaged the synchronic displacement of tyrosinase from melanosomes to lysosomes in B16 cells upon treatment with *Inulavosin* (Fig. 22). To further compliment this, the upregulation of tyrosinase in living cells – after Psoralen/Ultraviolet A (PUVA) addition – was visualised with **32**, and this increased concentration was confirmed by colourimetric assay. Although the detailed mechanism of displacement needs further inspection, **32** provides a straightforward perceptible method to investigate the metabolic breakdown of tyrosinase in cells and may be used within a clinical-setting for the treatment of tyrosinase-related diseases in the future.

Monoamine Oxidase-A (MAO-A) is an enzyme that catalyses the oxidation of monoamines, utilising oxygen during the process. MAO-A has an increased affinity for hydroxylated amines [98], and this fact was exploited by Wang and co-workers with the design of probe **33** (Fig. 21)**.** Expanding from a previously designed compound [99], probe **33** differs only by the length of the carbon-chain connecting the nitrogen atom to the 1,8-naphthalimide fluorophore [100]. Nevertheless, probe **33** displayed a remarkable fluorescence-intensity increase (186-fold) at 550 nm upon reaction with MAO-A. Probe **33** was able to detect endogenous MAO-A in living cells and zebra fish, demonstrating the potential for **33** to be employed in various biological systems.

6. Cytochrome P450

Cytochromes P450 (CYP) are a large family of enzymes containing heme as a cofactor and function as monooxygenases in phase 1 metabolism in mammals, with metabolism in humans being controlled by several sub families (including CYP1A2, CYP3A5, and CYP3A4). For example, cytochrome P450 1A (CYP1A) is an enzyme capable of dealkylation of aromatic hydrocarbons (Scheme 9) and has been shown to be responsible for conversion of pro-carcinogenic compounds into their carcinogenic forms among other functions [21]. Hence, detection and monitoring of CYP1A aids in the identification and evaluation of potential abnormalities that may arise in association with this important enzyme.

Ling *et al.* report their success in the synthesis of a fluorescent probe **34** (Fig. 23) that achieved the visualisation and detection of CYP1A activity [21]. The group synthesised a number of 1,8-naphthalimide analogues, however, **34** was found to possess heightened selectivity, efficient sensitivity and a ratiometric fluorescence change after sequential CYP1A-catalyzed *O*-demethylation (Scheme 10). The colour of the samples changed colourless to yellow, suggesting that **34** could function as a 'naked-eye' colourimetric indicator for CYP1A (Fig. 24). The considerable emission response coupled with a desirable bathochromic shift (112 nm) after the biotransformation implied that **34** could

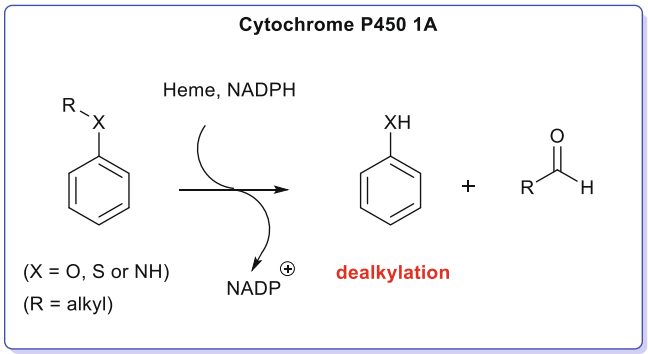

Scheme 9. The dealkylation of an aromatic alcohol, thiol or amine in the presence of CYP1A and NADPH.

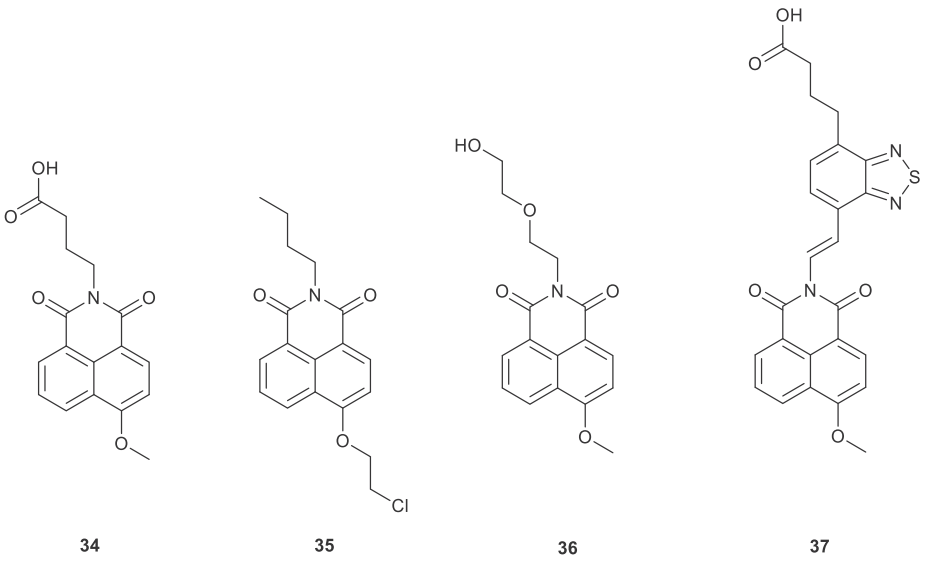

Fig. 23. Chemical structures of compounds **34**–**37**.

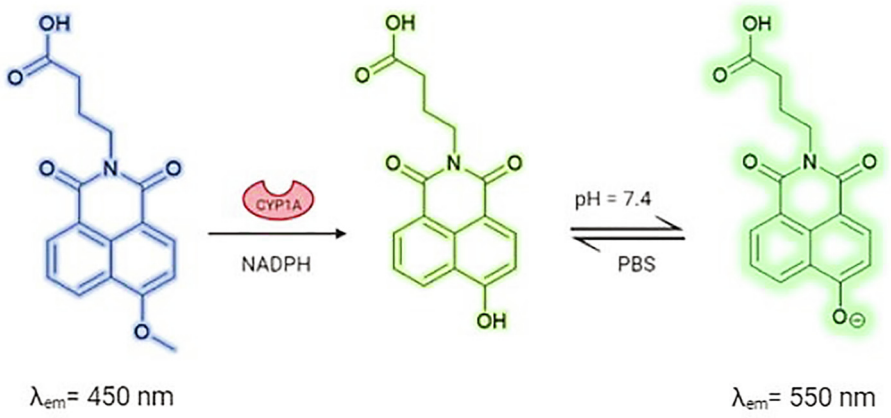

Scheme 10. General schematic for the conversion of 4-methoxynaphthalimide **34** to 4-hydroxynaphthalimide in the presence of CYP1A and fluorescence modulation based on pH.

function as a ratiometric probe to measure enzyme activity in biological samples.

Zhengjian and co-workers designed and synthesised a similar ratiometric fluorescent probe **36** (Fig. 23) for the detection of the human CYP1A enzyme [101]. However, in this case, the imide position of the naphthalimide was functionalised with a 2-(2-aminoethoxy) ethanol moiety. Similar to **34**, probe **36** was selectively dealkylated by CYP1A without interference from the other CYP enzymes.

Near-Infrared (NIR) probes (emission maxima between 650 and 900 nm) are attractive, due to their reduced photo-induced damage of sample, enhanced tissue penetration-depth, and marginal interference from auto-fluorescence [10,37]. The group of Li-Ying co-workers took advantage of this fact and designed a series of ratiometric chemo-sensors incorporating the 1,8-naphthalimide fluorophore for the CYP1A enzyme [102]. The inclusion of dichlorobenzene and benzothiadiazole (Probe **37**) acceptor groups onto the 'head' of the naphthalimide scaffold (Fig. 23) effectively increased the ICT distance and expanded the probability of the two-photon absorption (TPA) transition. The results from this investigation yielded interesting photoelectronic data regarding the fluorescent naphthalimide scaffold and may promote the synthesis of more efficient TPA fluorescent probes.

Building on their previous work, Ling *et al.* set out to devise an isoform-specific TPA fluorescent compound **35** (Fig. 23) for CYP1A1 based on the disparity between the 3D-structure and substrate [103]. The group demonstrated that by introducing a chloroethyl moiety they could achieve isoform-selectivity towards CYP1A1. Molecular docking simulations (Fig. 25) concluded that the establishment of a chloroethyl substituent arranged **35** into a more optimal position within the active site of CYP1A1, over that of CYP1A2. This suggested that probe **35**-*O*-dechloroethylation could transpire more promptly in CYP1A1.

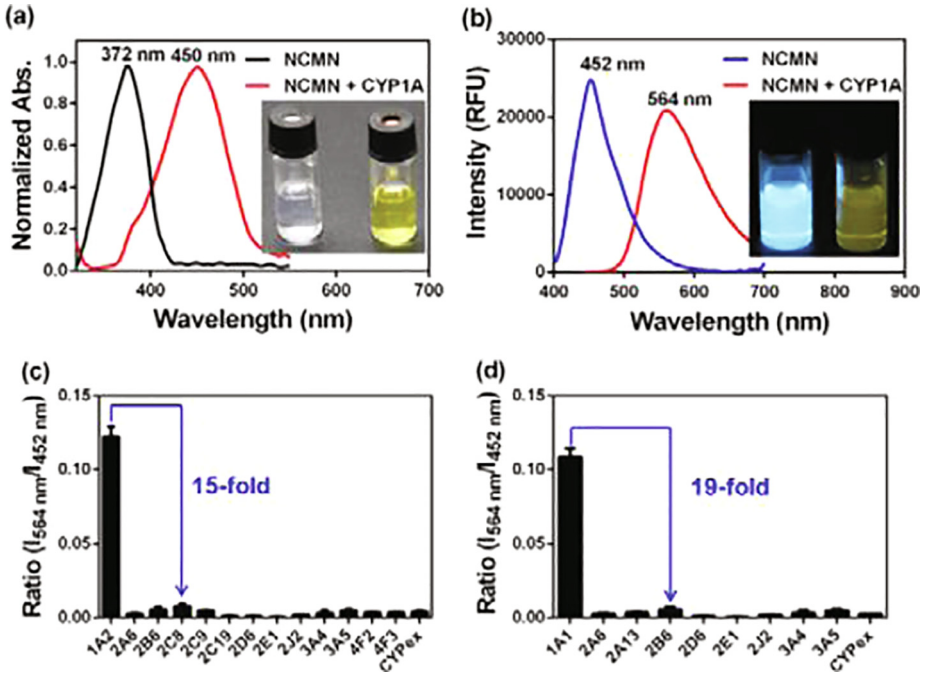

Fig. 24. (a) Absorption spectra of **34** ($20x10^{-6}$ M) with inclusion of CYP1A ($100x10^{-9}$ M). (b) Fluorescence emission spectra of **34** ($20x10^{-6}$ M) with inclusion of CYP1A ($100x10^{-9}$ M). Fluorescence feedback of **34** ($100x10^{-6}$ M) to different enzymes in human-liver microsome (c) and human-lung microsomes (d). Reprinted with permission from *J. Am. Chem. Soc.* **2015**, 137, 45, 14488–14495, *Copyright © 2015, American Chemical Society.*

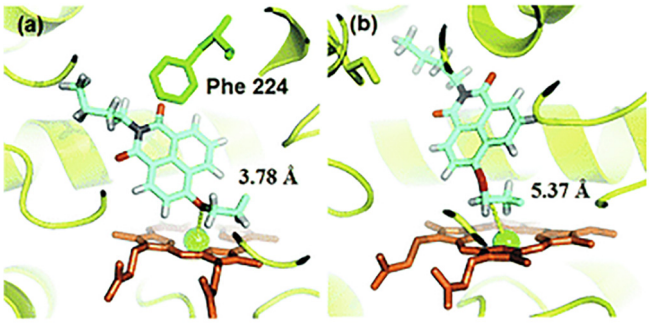

Fig. 25. Molecular docking simulations of **35** into CYP1A1 (a) and CYP1A2 (b). Reprinted with permission from *Chem. Sci.*, **2017**,8, 2795–2803, *Published by The Royal Society of Chemistry.*

7. Glycosidases

Glycosidases are enzymes of great interest due to their ability to carry out hydrolysis of a glycosidic bond (Scheme 11). Their ability to hydrolyse glycoconjugates resulting in the liberation of a fluorescent naphthalimide moiety is a method that has been exploited to enable targeted release of the fluorophore. Moreover, the use of a glycan unit to form glycoconjugates is highly advantageous as it gives rise to tumour cell targeting and increased solubility in aqueous media, deeming these probes highly valuable as chemosensors [104-108]. β-Glucuronidase (β-Glu) and β-Galactosidase (β-Gal) are two well-known members of this family of enzymes. β-Glu is known for its involvement in the degradation of endogenous and exogenous substances such as bilirubin and glucuronides found in exogenous drugs [109-111]. It is also known to be overexpressed in a variety of tumours such as colon carcinoma, renal carcinoma, as well as liver and prostate cancer; truly a valuable biomarker for disease [111]. β-Gal is involved in the hydrolysis of lactose to glucose and galactose [112]. More interestingly, it is a biomarker for a variety of ovarian cancers and cell senescence [113-115].

Gunnlaugsson, Scanlan and co-workers have recently synthesised a series of naphthalimide based probes consisting of a carbohydrate unit linked to a triazole naphthalimide moiety *via* a glycosidic bond [108]. Activation of the probes was achieved by hydrolysis of the glycosidic bond by either β-Glu or β-Gal. Compounds **38**–**41** (Fig. 27) were capable of rapid hydrolysis in the presence of the relevant glycosidase enzyme and furthermore, uptake of released the naphthalimide moiety could be observed by green fluorescence within the cytosol of the cell (Fig. 26). Such glycosidase activated probes will be useful for fluorescent imaging and for the delivery of 1,8-naphthalimides into tumour cell lines.

Gunnlaugsson, Scanlan and co-workers also reported the synthesis of glycosylated 4-amino-1,8-naphthalimide **43**, and related 1,8-naphthalimide-Tröger's base **44**. The capability of these compounds to perform as fluorescent probes for lectin binding was demonstrated where fluorescence modulations arose as a consequence of the disruption of aggregation. Binding studies carried out amongst other non-lectin proteins established that selective binding interactions between the α-mannoside probes and Concanavalin A (Con A) are responsible for the variations of luminescence; an approach that can be exploited for various biologically important applications (Fig. 28) [116].

A related paper investigated the self-assembly of **38**, **40**, and **42** possessing a 1,8-naphthalimide moiety and a glycan unit in protic polar media. This work demonstrated that these compounds can resemble the structure of larger biological matter and form luminescent self-assemblies. Using Helium-Ion Beam (HIB) (Fig. 29) and Scanning Electron Microscopy (SEM) techniques, the authors were able to confirm that compounds **38**, **40**, and **42** (Fig. 27) can manifest as spherical hierarchical self-assemblies. It was also shown using **42** that by cleaving the glycoside linkage altering of the compound can be achieved post-synthetically, and that glycosidase enzymes were capable of changing the morphological features of the self-assembly [13].

The group of Xiaochi synthesised probe **45** (Fig. 30) for the detection of β-Glu using a 4-hydroxy-1, 8-naphthalimide moiety. This probe exhibited fluorescence emission ratio changes from

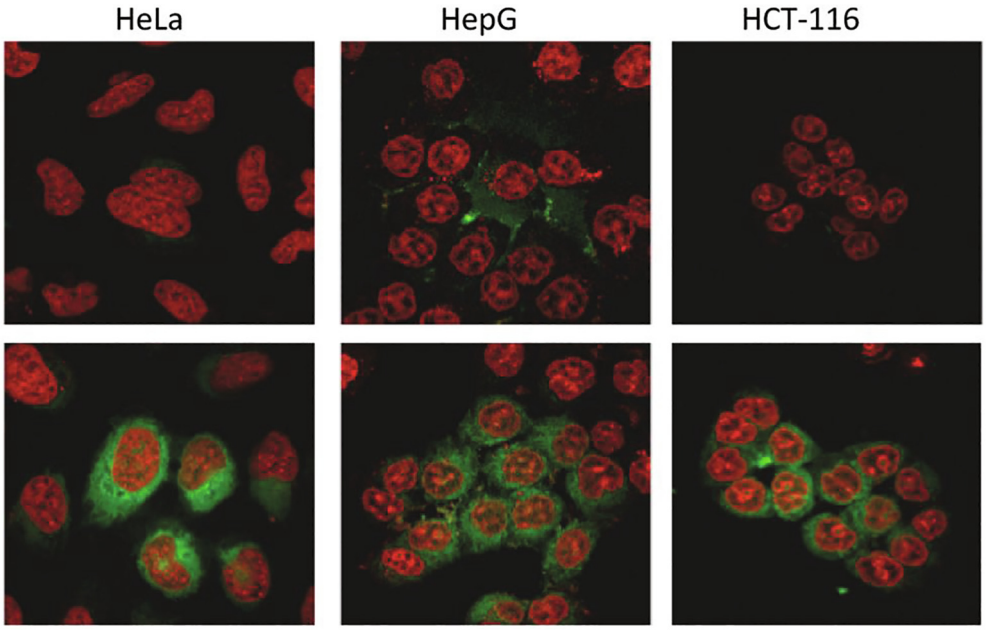

Fig. 26. Uptake of Probe **38** by cancer cells. Probe 1 incubated for 3 h at 0.1 mM concentration in cancer cell lines (first row). Second row shows the uptake of the naphthalimide after an incubation period of 3 h with cancer cell line and β-Gal for 1.5 h. Reproduced from *Chemical Communications* **2016**, *52*, 13086–13089 with permission from The Royal Society of Chemistry.

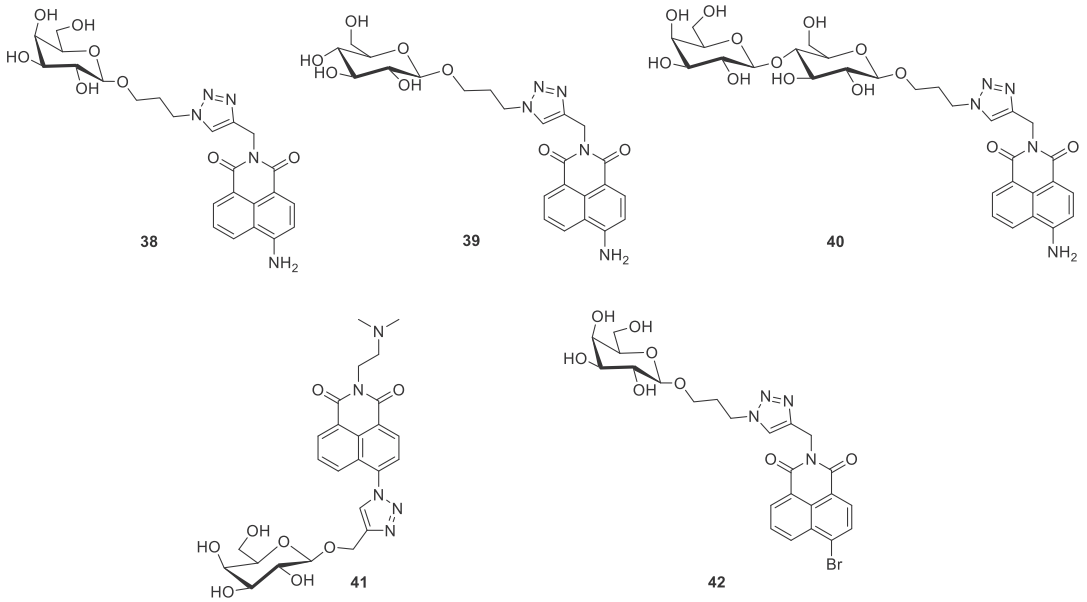

Fig. 27. Compounds **38**–**42**.

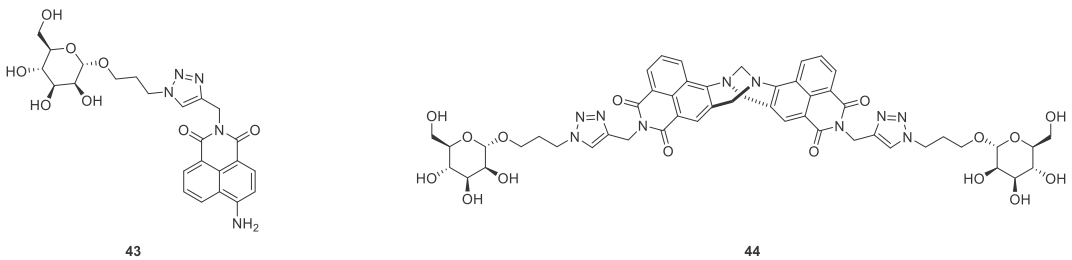

Fig. 28. Compounds **43** and **44**.

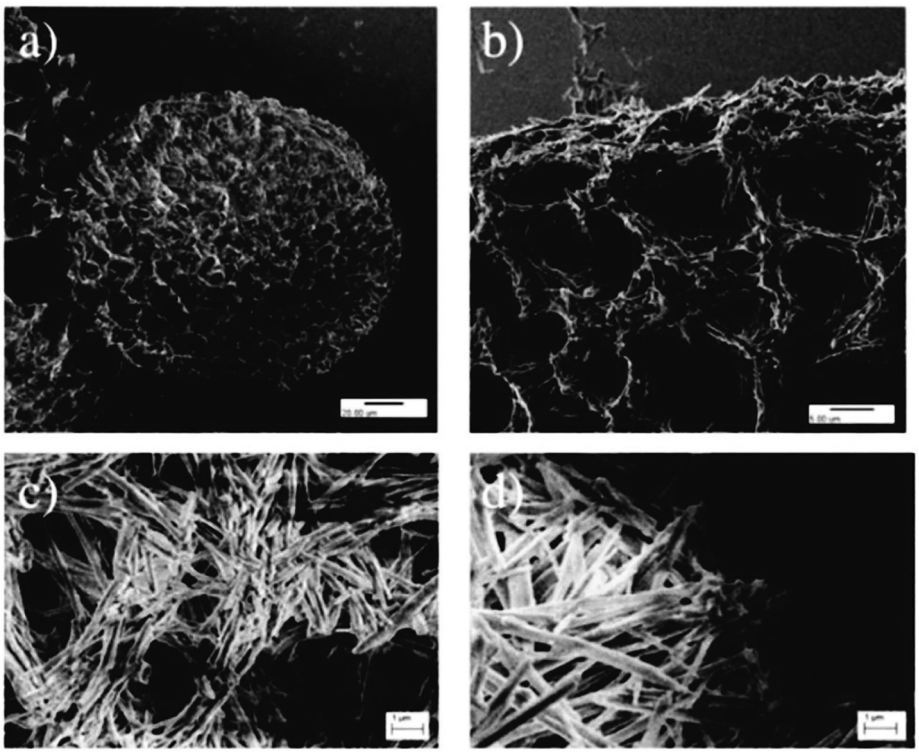

Fig. 29. Probe **38** HIB images consisting of glycosylated microspheres at varying concentrations in deuterated methanol. Reproduced from *Org. Biomol. Chem.*, 2020, **18**, 3475 with permission from The Royal Society of Chemistry.

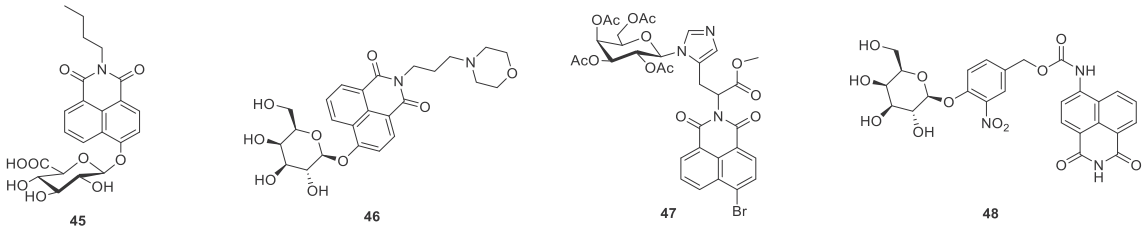

Fig. 30. Compounds **45**–**48**.

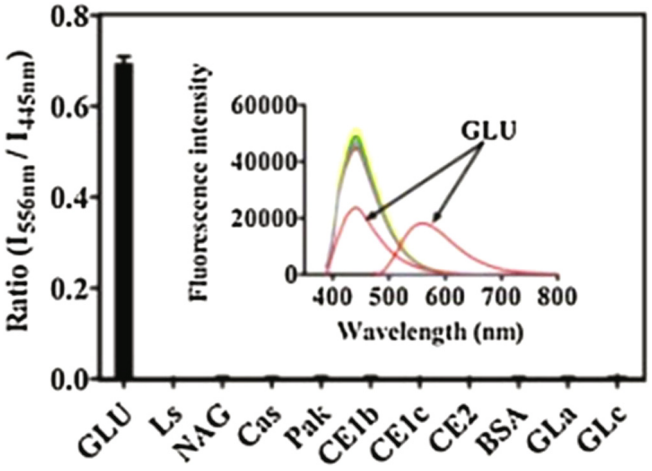

Fig. 31. Selectivity of **45** in the presence of other hydrolase enzymes, and fluorescence emission at 558 nm and 450 nm after incubation for 30 min with GLU (10 μg/mL). Reprinted from *Sensors and Actuators B*: Chemical, Volume 262, Xiaokui Huo, Xiangge Tian, Yannan Li, Lei Feng, Yonglei Cui, Chao Wang, Jingnan Cui, Chengpeng Sun, Kexin Liu, Xiaochi Ma, A highly selective ratiometric fluorescent probe for real-time imaging of *β*-glucuronidase in living cells and zebrafish, Pages 508–515, Copyright 2018.

blue to yellow-green upon sensing β-Glu, while no response was observed in the presence of common hydrolase enzymes and other endogenous substance (Fig. 31). **45** was applied for imaging of β-Glu in HepG2 (liver cancer cell line) and LoVo (colon cancer cell line), which indicated that β-Glu activity in HepG2 cells was much greater than that of LoVo cells. Moreover, **45** was capable of detecting β-Glu in living cells, tumour tissues and zebrafish. Based on their results it was suggested that **45** could be a sensitive and selective molecular probe for cancer diagnosis [111].

Wang *et al.* synthesised a two-photon fluorescent compound **46** (Fig. 30) based on the 1,8-naphthalimide moiety, again taking advantage of the β-galactose moiety for detecting the β-Gal enzyme. The morpholine ring was also an important part in the design allowing for lysosome localisation. Upon enzyme activation and cleavage of the β-galactose a fluorescence enhancement at 560 nm was observed with a blue to green fluorescence shift (Scheme 12). The highly sensitive probe **46** could be exploited to image endogenous β-Gal with a strong green fluorescence observed with both one and two photon fluorescence imaging in human ovary carcinoma SKOV-3 cells. Furthermore, merging of fluorescence images of the probe with a lysosome targeting dye (LysoTracker Red DND-99) demonstrated the ability of **46** to image β-Gal within lysosomes [117].

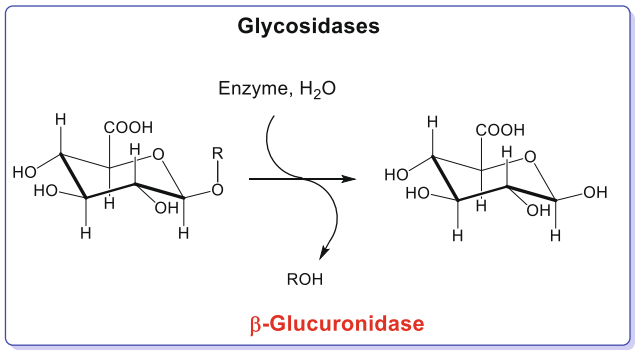

Scheme 11. The hydrolysis/ glycosidic linkage cleavage of a glycan moiety in the presence of relevant Glycosidase.

Martínez-Máñez *et al.* reported a two-photon probe **47** (Fig. 30) for the detection of cell senescence. The probe consisted of an acetylated galactose linked to a 1,8-napthalimide fluorophore via an L-histidine methyl ester linker. The probe displayed a 10-fold fluorescence enhancement at 540 nm in senescence induced human melanoma cell line SK-MEL-103, with an absence of fluorescence in control SK-MEL-103 cells treated with **47**. This fluorescence enhancement being attributed to the hydrolysis of **47** to the free L-histidine methyl ester naphthalimide reporter. Furthermore, detection of senescence was achieved *in vivo* using tumour bearing mice treated with *Palbociclib* (senescence inducer). Upon intravenous injection of 8 in mice a 15-fold fluorescence enhancement was observed in tumours after 3 h of treatment. It was also observed that **47** localises selectively in senescent tumours amongst other organs (Fig. 32) [118].

Shicong and co-workers reported the development of three fluorescent probes for the sensing of β-Gal in aqueous media. These probes were shown to be responsive to β-Gal as a result of the blue to green fluorescence emission, and also established cellular localisation and low cytotoxicity. One probe in particular, probe **48** (Fig. 30), proved to be highly sensitive to β-Gal noted by its fluorescence response, with a low detection limit in PBS buffer (0.17 U L^{-1}). This probe was also capable of two-photon fluorescence imaging which may render it a useful compound to aid in studying the functions and mechanisms of β-gal [115].

8. Transferases

Transferases are another family of enzymes in which 1,8-napthalimides have been exploited as fluorescent probes. Transferases are capable of transferring a specific functional group (e.g. a methyl or glycosyl group) from a donor molecule to an acceptor molecule (Scheme 13). For example, within the liver and endoplasmic reticulum, uridine diphosphate glucuronosyltransferases enzymes (UGTs) are responsible for the transfer of a glucuronic acid moiety from the donor uridine diphosphate-glucuronic acid (UDPGA) to an acceptor. UGTs are involved in many cellular metabolic pathways including metabolism of bilirubin and some clinical drugs such as the chemotherapeutic agent etoposide. Moreover, it has been noted that many clinical drugs may inhibit the rate of glucuronidation of UTG1A1 substrate drugs and endogenous substances such as bilirubin [119-122]. The Glutathione S-Transferase (GST) family of enzymes also play a vital role in the detoxification of many endogenous substances such as secondary metabolites produced during oxidative stress as well as a variety of chemical carcinogens [123]. Fluorescent probes for GST can be useful to determine drug induced liver damage and, furthermore, GSTP1 has been reported as a biomarker known to be upregulated in several cancer tissues [124-126].

Taking advantage of these facts, Yang and co-workers developed a ratiometric fluorescent probe for the detection of human UDP-glucuronosyltransferase 1A1 (UGT1A1). Probe **49** (Fig. 33), a 4-hydroxy-1,8-naphthalimide bearing a carboxylic substituent underwent 4-O-glucuronidation in the presence of UGT1A1 and UDPGA, with an observed fluorescence enhancement of the glucuronidated probe at 450 nm. High fluorescence intensity ratios (26-fold) were achieved by **49** amongst other UGT enzymes such as UGT1A8 and UGT1A10. A linear relationship for the fluorescence

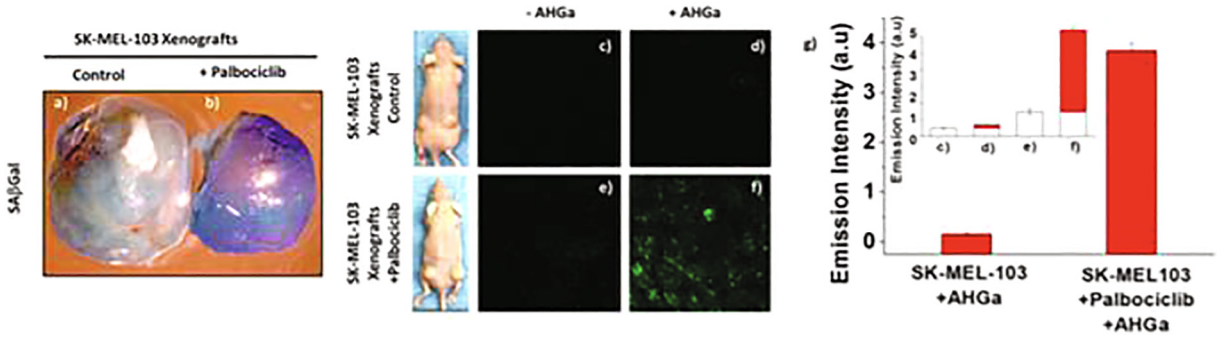

Fig. 32. (a) SK-MEL-103 control tumours. (b) SK-MEL-103 senescent tumours after SaβGal staining. SK-MEL-103 tumours (c,d) SK-MEL-103 senescent tumours (e,f). Absence of probe **47** (c,e). Intravenous tail injection of probe **47** (d,f). Fluorescence intensity measurements (g). Reprinted with permission from *J. Am. Chem. Soc.* 2017, 139, 26, 8808–8811. Copyright 2017 American Chemical Society.

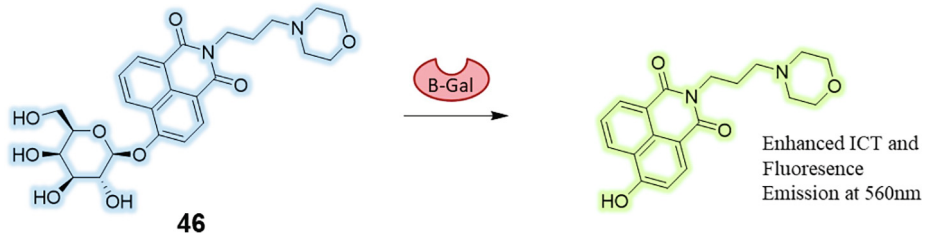

Scheme 12. Hydrolysis mechanism of β-Gal. Hydrolysis of Probe **46** to liberate a 4-hydroxynaphthalimide moiety.

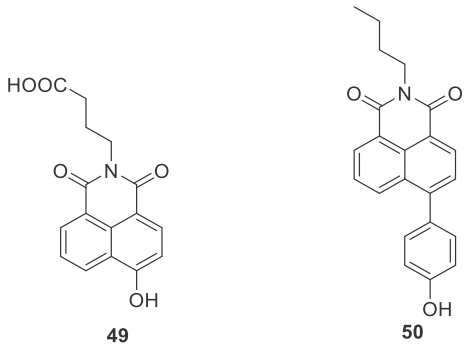

Fig. 33. Probes **49** and **50.**

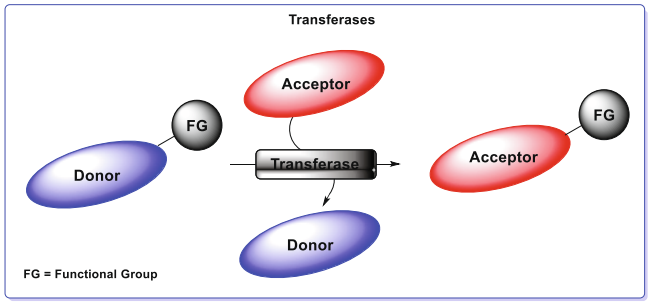

Scheme 13. Schematic representation of transfer of a functional group from a donor molecule to an acceptor in the presence of a transferase enzyme.

ratio (I_{450}/I_{564}) with increasing concentration of the UGT1A1 in the presence of **49** was observed. Furthermore, esterification of **49** allowed for facile uptake in HepG2 cells (via endogenous esterases) where the glucuronidated probe **49** displayed an intense blue fluorescence exhibiting its potential as a ratiometric fluorescent probe for human UGT1A1 *in cellulo* [127].

Yang *et al.* also developed probe **50** (Fig. 33) for the sensing of uridine diphosphate glucuronosyltransferase 1A1 (UGT1A1). Probe **50** consisted of *N*-butyl-4-phenyl-1,8-naphthalimide with a phenolic group on the 4-position which established PET quenching. Turn on fluorescence of **50** relied on O-glucuronidation which dramatically enhanced its fluorescence emission at 520 nm in the presence of UGT1A1 and co factor uridine diphosphate-glucuronic acid (UDGP) (Scheme 14). **50** displayed high sensitivity

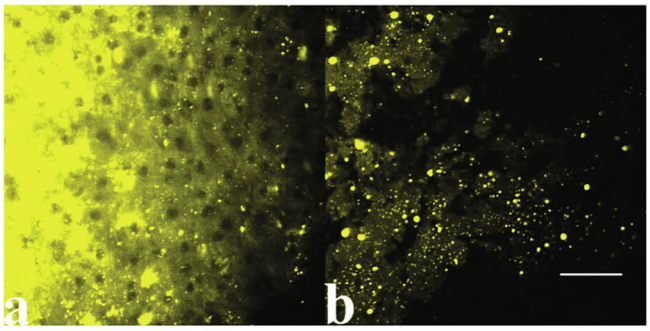

Fig. 34. Two-Photon fluorescence visualisation of drug induced liver injury samples. Reprinted with permission from *Anal. Chem*. 2017, 89, 15, 8097–8103. Copyright 2017 American Chemical Society.

and selectively for UGT1A1 under complex physiological conditions and was also capable of monitoring the activity of UGT1A1 in HepG2 cells (which show high expression of UGT1A1). Furthermore, **50** was capable of binding at the same enzymatic site as bilirubin, proving reliable for real time analysis of UGT1A1 in biological samples [128].

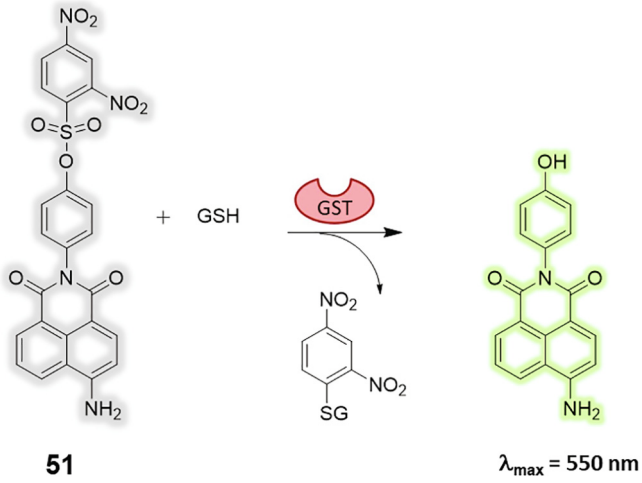

Scheme 15. The reaction of Probe **51** acting as a donor molecule in the transferase reaction of a 2,4-dinitrobenzenesulfonate with GST.

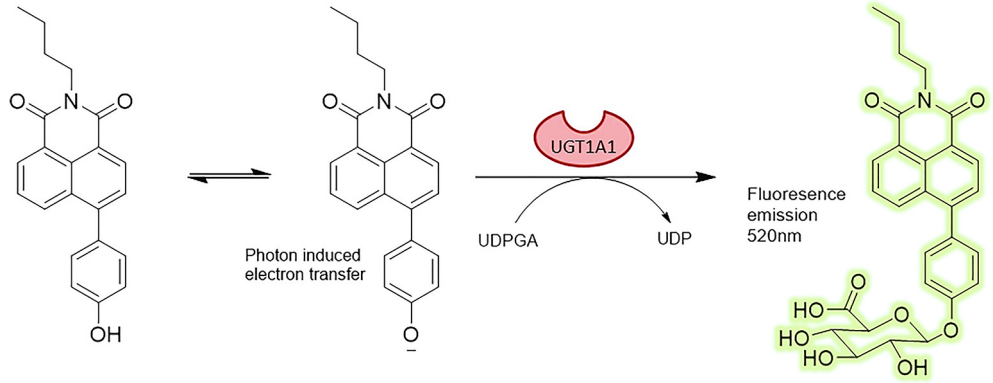

Scheme 14. O-glucuronidation of Probe **50**.

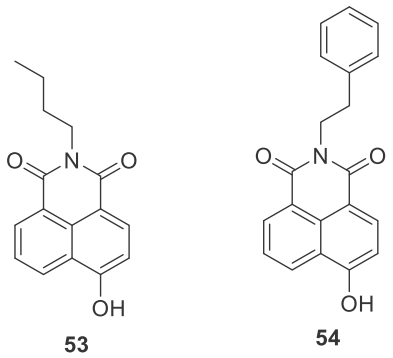

Fig. 35. Chemical structures of probes **53** and **54.**

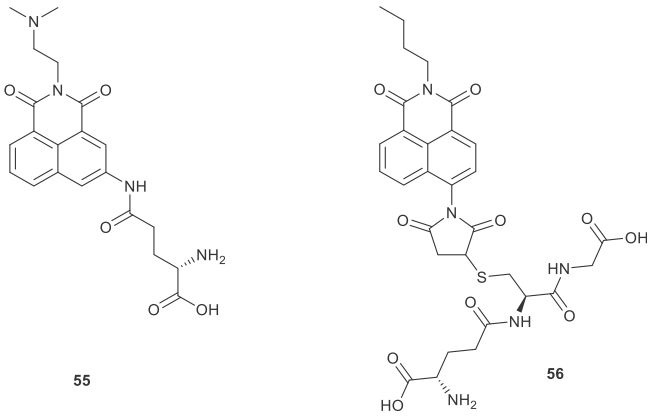

Fig. 37. Chemical structures of compounds **55** & **56**.

Feng *et al.* reported the design of an "off–on" two-photon (TP) probe **51** (Scheme 15) featuring, a 2,4-dinitrobenzenesulfonate (Glutathione S-transferase (GST) substrate unit and quencher) and a 1,8-naphthalimide derivative (fluorophore). **51** exhibited an absorption peak at 450 nm and showed no fluorescence emission in the absence of GST. However, upon addition of GST (Scheme 15), the absorbance maximum was blue-shifted to 437 nm and an increase in fluorescence intensity (40-fold) was achieved, with a 35 ng/mL detection limit. **51** was highly selective for GST in comparison to other relevant biological species Successful confocal microscopy of **51** allowed for the imaging of GST in cells and Drug-induced liver injury (DILI) samples (Fig. 34), demonstrating that **51** may be used as a promising practical diagnostic in biological samples [129].

Fujikawa *et al.* also reported the use of a naphthalimide based probe, **52** (Scheme 16) as a fluorogenic substrate for GST. In the presence of GSTP1-1 and GSH a significant fluorescence enhancement (837-fold) is observed at 503 nm as a result of thiolate reacting at the *ipso* carbon atom, replacing the bromo group. **52** was shown to be non-reactive in the presence of various redox species. Furthermore, **52** was capable of visualising GST activity in live cells seen by visually clear green fluorescence output primarily being activated by GSTP1, **52** also proved itself capable of differentiating between cancer cells (fibrosarcoma HT1080 cells that express endogenous GSTP1) and normal cells (HT1080 cells with RNAi treatment to suppress GSTP1). They also showed that derivatives of the 4-bromo-1,8-naphthalimide with different substitution at the imide site (such as ethyl, phenyl, hydroxyethyl or p-benzoic acid) were useful for imaging of GSTP1 in live cells [130].

Naphthalimides have also been exploited as probes for another class of transferases, glucosyltransferases. Ma and co-workers synthesised a probe capable of detecting glucosyltransferases (GTs) in Fungi. Probe **53** (Fig. 35) was simply a *N*-butyl-4-hydroxy-1,8-naphthalimide in which the 4-position could accept a glucosyl group. By increasing the concentration of GT in the presence of UDGP, emission of **53** at 556 nm decreased while emission at 446 nm increased upon glucosylation under physiological conditions. While **53** showed high sensitivity, it also achieved high selectivity amongst various glycosyltransferases and glycoside hydrolases. Furthermore, blue fluorescence was observed under UV light when **53** was incubated with several fungal strains owing to the GTs present in *R. oryzae* and *M. citcinelloides*. Two photon fluorescence imaging (λ_{ex} = 800 nm) showed an even greater fluorescence intensity output [131].

James *et al.* synthesised a fluorescent probe **54** (Fig. 35) for the detection of *Streptococcus mutans* glucosyltransferase which is known to play a key role in tooth decay. **54** consisting of a *N*-phene thyl-4-hydroxy-1,8-naphthalimide moiety that could accept a glucosyl group from uridine-diphosphate glucose (UDPG) in the presence of Glucosyltransferase (GTF). A linear relationship of fluorescence ratio (I_{440}/I_{560}) was observed with increasing concentrations of GTF, with selectivity established for GTF amongst other glycosidases and hydrolases. Upon incubation of **54** with different strains of bacteria it was noted that blue fluorescence observed in *Streptococcus mutans* had the highest level of GTF expression (Fig. 36). Furthermore, **54** was applied as a screening method for the evaluation of epigallocatechin gallate and gallocatechin gallate as potential inhibitors of GTF's [132].

γ-Glutamyl transferase (GGT) is one of the many amino acyltransferases that act on amine functionalities to transfer peptide bonds. GGT is an enzyme which selectively catalyses cleavage of the γ-glutamyl bond of glutathione (GSH). Various cancer cell-

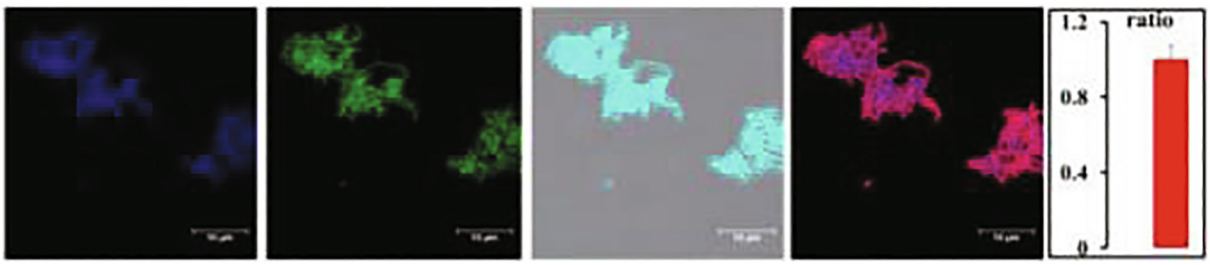

Fig. 36. Fluorescence images of *Streptococcus mutans*. Glucosylated probe **54** (λex = 405 λem = 415–465 nm) (left), Probe 6 (λex = 405 λem = 535–585 nm) (middle left), Merged image (centre), Fluorescence ratio ($I_{415-465}/I_{535-585\ nm}$) (middle right) (right). Reproduced from *Chem. Commun.*, 2019, **55**, 3548. Published by The Royal Society of Chemistry.

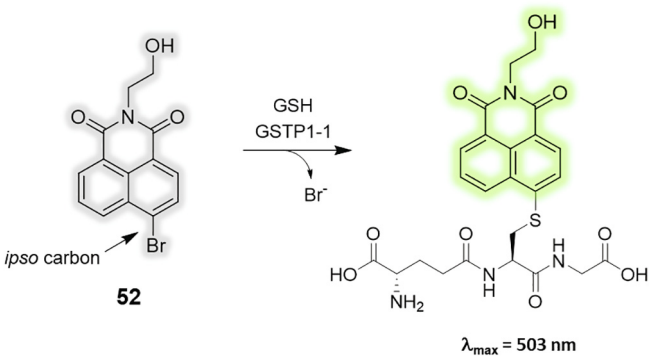

Scheme 16. Nucleophilic aromatic substitution of **52** at the ipso carbon.

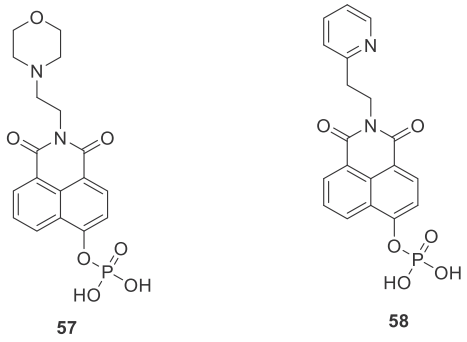

Fig. 38. Probe **57** and **58**.

lines have been described that overexpress GGT, allowing this enzyme to be recognised as a possible cancer biomarker [133]. With this in mind, Guo and co-workers reported a sequential ICT-reactive probe **55** (Fig. 37), for the detection of DNA deterioration in cancer cells [134]. GGT and *N*-acetyltransferase (NAT) were chosen as the recognition target because GGT & NAT are upregulated in cancer and in localised regions of tarnished DNA, respectively. L-Glutamate (Glu) and an imino group (at the 5-position) were utilised as the enzyme substrate. In its latent state, **55** displays blue fluorescence (441 nm), which remains stagnated on the cell-surface due to its hydrophilicity. However, the cell-membrane-bound GGT enzymatically cleaves the Glu-unit, and **55** emits a green fluorescence (531 nm) due to the initial ICT mechanism (Scheme 10). Subsequently, the amino-group in the 5-position of the fluorophore is acetylated by NAT to give –NH–CO–CH_3. Now localised in regions of DNA damage, a blue fluorescence (455 nm) signal is seen again due to the manifestation of the second ICT mechanism.

Many of the market-available GGT probes – designed using the direct conjugation of a γ-glutamyl group – generally have slow enzyme kinetics due to the rather large fluorophore being in close proximity to the enzyme's specificity pocket [135].

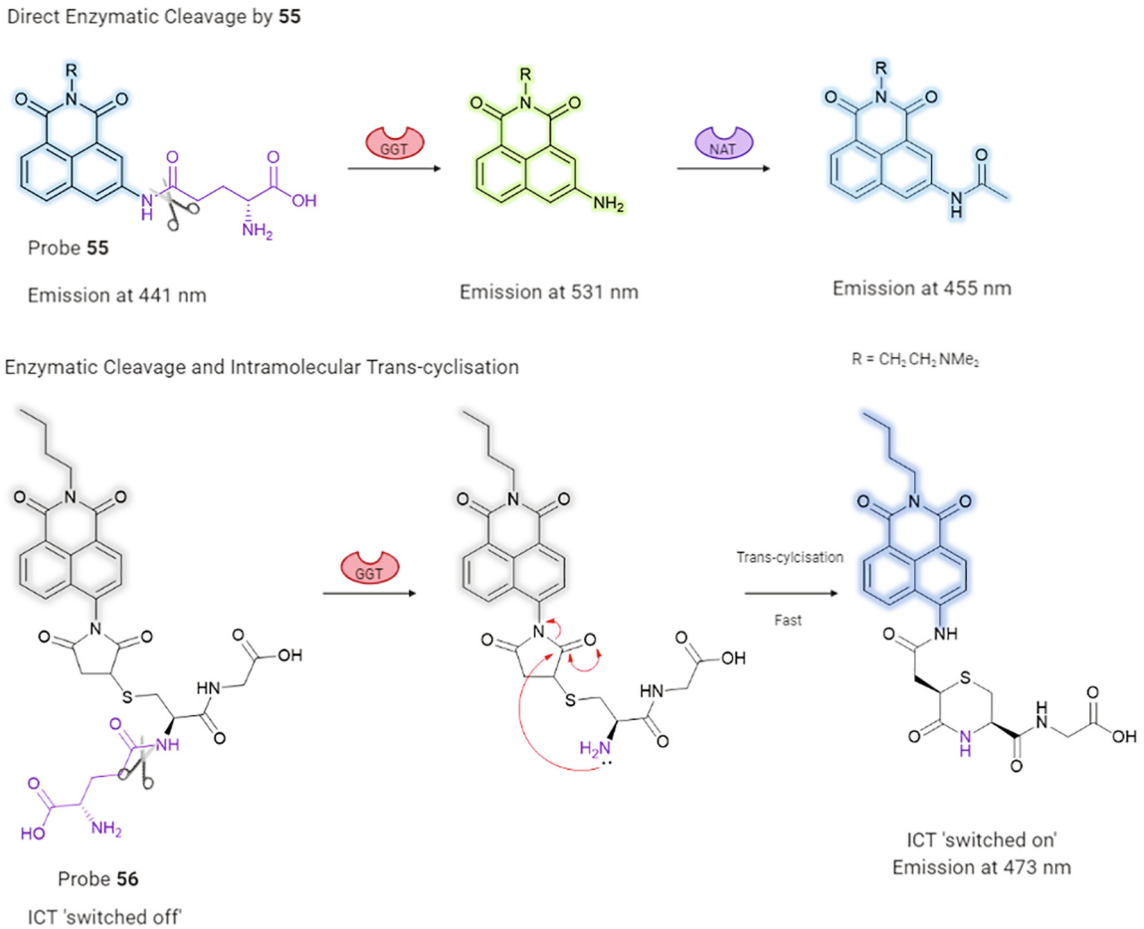

Scheme 17. Comparison of direct enzymatic cleavage approach versus the transcyclization method.

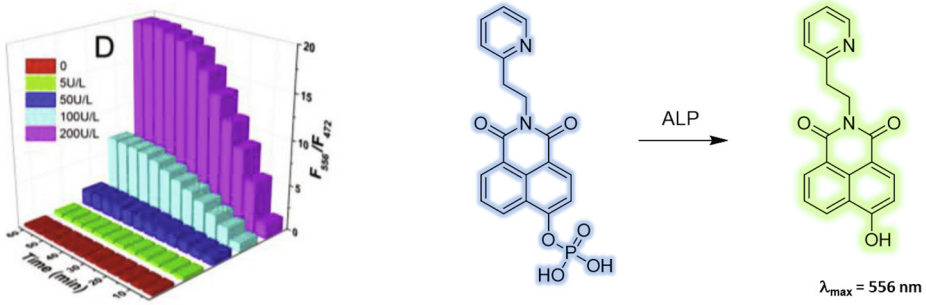

Fig. 39. (Left) fluorescence intensity ratio *vs.* time of **58** (10 mM) in the presence of different activity of ALP (colour coded) λ_{ex} = 425 nm. (Right) Schematic representation of the sensing mechanism of **58** in the presence of ALP. Reprinted from *Analytica Chimica Acta*, Volume 1066, Congcong Gao, Shunping Zang, Longxue Nie, Yong Tian, Rubo Zhang, Jing Jing, Xiaoling Zhang, A sensitive ratiometric fluorescent probe for quantitive detection and imaging of alkaline phosphatase in living cells, Pages 131–135, Copyright 2019, with permission from Elsevier.

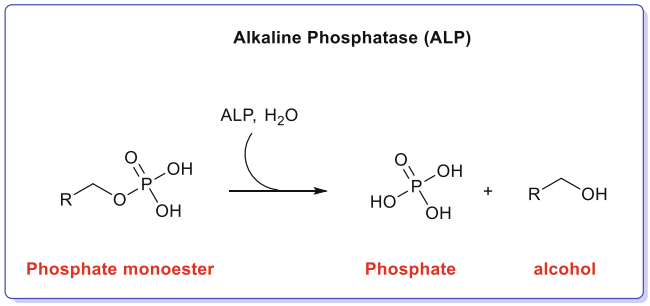

Scheme 18. The hydrolysis/ dephosphorylation of phosphate monoester to phosphate in the presence of ALP.

Probe **56** (Fig. 37) reported by Wang et al. [136] took advantage of a *trans*-cyclisation cascade reaction (Scheme 17). This method facilitates the installation of a cumbersome fluorophore abroad from the active site to boost the probe's kinetic rate. In turn, this facilitated rapid *in situ* detection of GGT activity. Initiated by the cleavage of the γ-glutamyl group, the reaction results in the formation of a six-membered thiomorpholinone ring. The *trans*-cyclised product exhibited a fluorescence increase of more than 200-fold (at 473 nm), with a detection-limit equal to 0.21 mU/mL. Notably, when compared to other probes based on the 1,8-naphthalimide fluorophore, **56** does not contain a free amino group after enzymatic cleavage. This conveniently excludes conceivable issues that may arise from the interaction of other

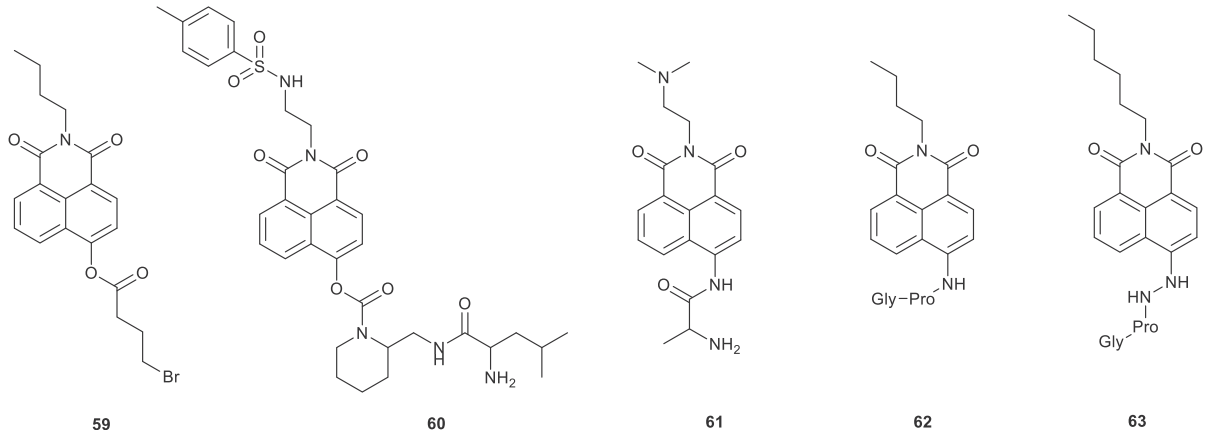

Fig. 40. Chemical structures of compounds **59**–**63**.

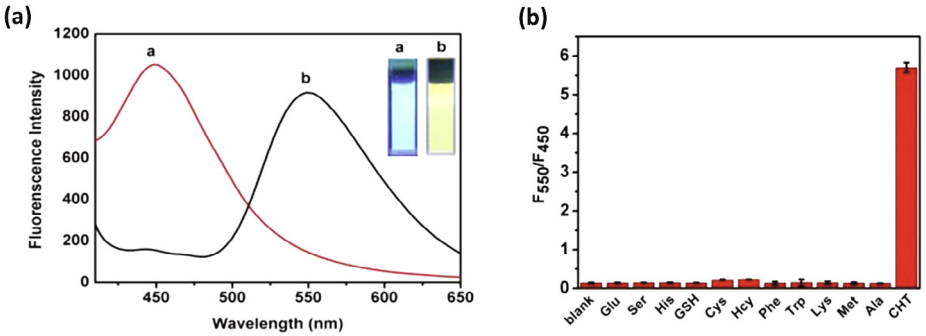

Fig. 41. (a) Absorption and fluorescence emission spectra of **59** (10 μM) after reaction with CHT. (b) Fluorescence response of **59** (10 μM) to amino-acids and bio-thiols in HEPES buffer. Reprinted with permission *from Sensors & Actuators: B. Chemical* (**2018**) 204–210, *Copyright © 2018 Elsevier B.V. All rights reserved.*

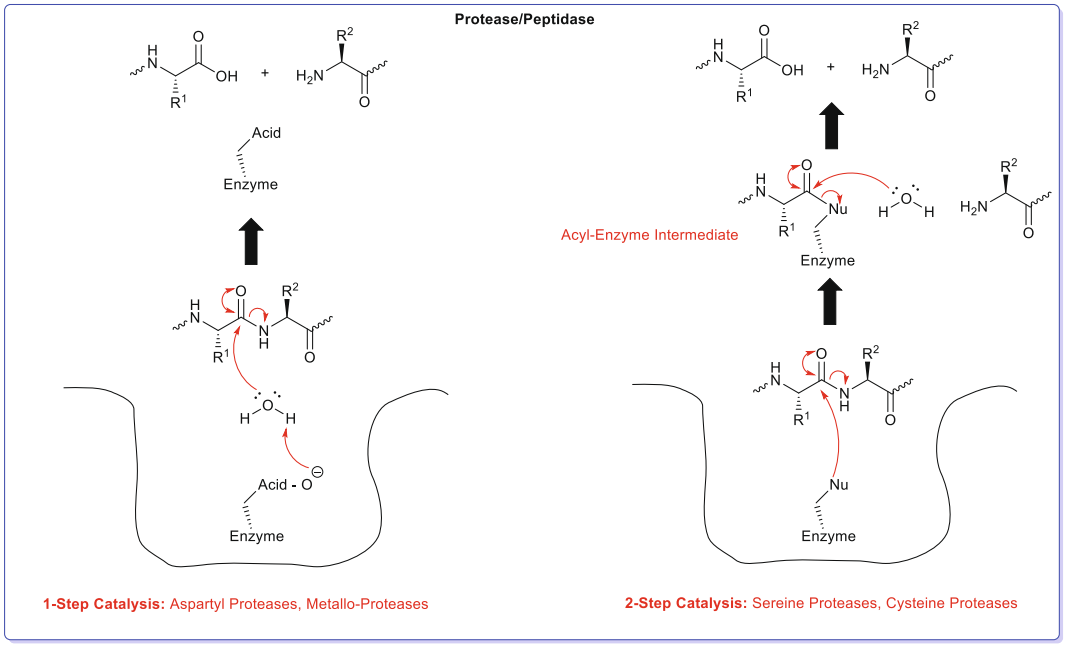

Scheme 19. Mechanisms of peptide bond cleavage associated with protease/peptidase activity.

enzymes, which can frequently lead to arduous time-dependent fluorescence responses.

9. Alkaline phosphatases

Alkaline phosphatase (ALP) is a hydrolase enzyme involved in the hydrolysis/dephosphorylation of a wide range of phosphorylated biomolecules (Scheme 18) [137]. Atypical levels of ALP are characteristic of several cancers (e.g. bone and prostate cancers) as well as osteoporosis and hepatitis, rendering ALP another valuable biomarker for medical diagnostics [138-142].

Bhuniya and co-workers synthesised probe **57** (Fig. 38) capable of detecting lysosomal phosphatase by hydrolytic cleavage of a phosphate moiety at the 4-position. In the presence of phosphatase, a fluorescence enhancement of 45 fold was observed at 560 nm (blue to yellow fluorescence) as well as an expected red shift in the absorption spectra from 370 nm to 450 nm. **57** displayed a low detection limit of 1.2 ng/mL towards phosphatase as well as a high selectivity in comparison to other biologically relevant analytes such as glutathione, ascorbic acid, and cysteine. **57** also proved useful in the detection of phosphatase both intracellularly and extracellularly in LNCap cells (prostate cancer cell line) where localisation was to lysosomes as a result of the lysosomal targeting moiety at the imide site [31].

Zhang et al. reported the use of a naphthalimide based ratiometric fluorescent probe **58** (Fig. 38) capable of detecting ALP as a result of the phosphate moiety at the 4-position. Upon hydrolysis of the phosphate a change in fluorescence from blue to a strong green emission at 556 nm was observed. The probe displayed excellent specificity for ALP where a dramatic fluorescence change was observed in comparison to other enzymes such as carboxylesterase and β-D-Glucosidase. Additionally, **58** showed green fluorescence in HepG2 cells in which ALP is overexpressed. This intense increase in emission is thought to be a result of the ICT characteristics of the liberated naphthalimide and further exemplifies the usefulness of naphthalimides in monitoring and detecting endogenous ALP activity (Fig. 39) [143].

10. Proteases and peptidases

Proteases play a crucial role in coordinating many physiological processes from the digestion of food to blood clotting. Moreover, recent reports suggest their implication in various cancers, including hepatocellular, prostate, and pancreatic carcinomas (Scheme 19). Proteases belong to a group of hydrolases in which they facilitate the breakdown of peptide bonds in proteins (Scheme 19). In general, proteases fall into 4 distinct categories, each with their own corresponding mechanistic process: Aspartyl, Metallo-, Cysteine and Serine proteases. Within the active-sites of cysteine and serine protease, the corresponding residue is adjacent to an electron-withdrawing group, this promotes nucleophilic attack on the peptide bond. In the case of aspartyl and metalloproteases, a molecule of H_2O is "activated" to serve as the nucleophile instead of the enzyme itself [146]. Although different classes of protease(s) exist, the process of peptide-bond cleavage is generally the same. The design of fluorogenic probes that target proteases can be attained by assimilating specific amino acid sequence(s) or peptidomimetics as concealing groups or linkers. The recognition sequences of protease enzymes can vary, with some ranging from one amino acid, to over 20 [6].

Many protease-activated probes have been recorded in the literature [147,148]. However, until recently, examples that exploit a 1,8-naphthalimide as the fluorescent core have remained scarce. Nanyan *et al.* have designed a ratiometric fluorescent probe **59** for the detection of Chymotrypsin (CHT) by assimilating a 4-bromobutyryl group into the fluorescent scaffold of the 1,8-naphthalimide core (Fig. 40) [149]. CHT enzymatically removes the 4-bromobutyryl substituent from the naphthalimide and dramatically transforms its photophysical properties, thus achieving ratiometric detection of CHT. The acuteness of **59** was examined against metal ions, anions, biomolecules, and common enzymes.

The investigation showed no significant fluorescent changes, except for trypsin. Moreover, **59** displays high binding affinity and catalytic efficiency (detection limit = 8.4 ng/mL) against CHT (Fig. 41) [149].

Endoplasmic Reticulum Aminopeptidase 1 (ERAP1) plays a crucial role in antigen transformation, and ERAP1 disturbance has shown to be implicated in various diseases [150]. This makes monitoring its activity an efficient method for disease diagnosis and treatment. To this end, Weihong and co-workers report the synthesis of probe **60,** which utilises L-leucine as a trigger moiety and a methyl sulphonamide (Scheme 20) as an ER-targeting scaffold for visualising ERAP1 activity [151]. **60** displayed impressive sensitivity to ERAP1, boasting a 95-fold fluorescence increase at 550 nm. Interestingly, the authors demonstrated that **60** can be used to oversee discrepancies in ERAP1 under particular conditions. HeLa cells that were treated with IFN-γ showed increased amounts of ERAP1, which were monitored by **60**. It was also demonstrated, that after the treatment of HeLa cells with *N*-ethylmaleimide or dithiothreitol, **60** was able to show the changes in the ER by visualising the activity of ERAP1. These results showcased the ability of **60** to expose ERAP1-related diseases.

Not unlike ERAP1, aminopeptidase N (APN) has become an important biomarker for the diagnosis and prognosis of various cancers, including colorectal cancer and ovarian cancer [152]. Moreover, it has been established that APN holds an integral position as an indicator for cancer stem cells, thus becoming of interest as a target for the construction of fluorescent probes [153]. An approach reported by Fang et al. [154] incorporated the 1,8-naphthalimide fluorophore, and alanine/norvaline as the trigger moieties. Of the more promising probes, **61** (Fig. 40) showed a distinct shift from 460 nm to 550 nm, and the ratio of fluorescence intensities increased from 0.45 to 4.67 after 50 min incubation with porcine APN (0.2 IU). Notably, ES-2 cells incubated with both **61** and *Bestatin* (inhibitor), exhibited blue nuclear fluorescence but largely quenched green fluorescence in the cytoplasm. The significant differences in fluorescence responses demonstrated that probe **61** may be employed for visualising APN in living cells.

Another protease enzyme that has received a lot of attention recently is dipeptidyl peptidase IV (DPPIV), a serine protease with roles in endocrine control and cell metabolism, amongst others [155]. The pervasive expression and activity of DPPIV allows the enzyme to contribute to physiological processes, such as the governance of glucose metabolism. Thus, DPPIV has been employed as a treatment of type 2 diabetes. It has also been shown to serve as a receptor for Middle East respiratory syndrome (MERS) coronavirus infection [156]. This evidence suggests that a disturbance in the level of DPPIV may provide insight into the early diagnosis of DPPIV-related diseases [157]. Guang-Bo Ge and co-workers reported a novel 1,8-naphthalimide-containing fluorescent probe **62**[157] for the detection of DPPIV in organic systems. One of the main advantages of **62** was its excellent two-photon properties (Fig. 42) and the fact that it could be excited with NIR-light. The authors demonstrated that **62** could measure endogenous DPPIV in kidney tissue (murine) by utilising confocal microscopy under laser excitation at 805 nm. Similarly, the group of Dimitrova designed an enzymatic-probe **63** for detecting DPPIV with naphthalimide as its fluorescent core [158]. However, probe **63** exploited the enzyme's ability to hydrolyse hydrazide bond(s) as its trigger moiety. Like probe **62**, **63** was applied in tissue sections of rat and mouse organs to reveal the location(s) of DPP IV. These findings suggest that both probes (**62**, **63**) may be adapted for use in living systems, to measure and investigate endogenous DPPIV activity.

11. Hydrolases

Hydrolases are a class of enzyme that utilise water to catalyse the cleavage of covalent bonds (Scheme 21). They are a broadly classified family of enzymes that include many subtypes such as lipases, phosphatases, glycosidases, peptidases and nucleosidases to name just a few and they are ubiquitous in nature [159]. It is of no surprise then, that hydrolases are prominent targets of enzyme-activated fluorogenic probes.

Han et al. designed a naphthalimide-based probe **64** capable of the detection of S-adenosylhomocysteine hydrolase (SAHase) [160]. The probe consisted of a 1,8-naphthalimide moiety linked to an adenosine moiety *via* a thioether bond which underwent hydrolysis in the presence of the enzyme (Scheme 21). PET quenching of the 1,8-naphthalimide fluorophore was facilitated by the adenosine moiety but gave rise to a fluorescence enhancement (10-fold) at 470 nm in the presence of SAHase. The response was a proportional relationship between fluorescence intensity and SAHase concentration. **64** also showed great selectivity amongst relevant biological species and other hydrolases. Moreover, green fluorescence was observed in HL-60 human promyelocytic leukaemia cells due to activation of **64** by SAHase. Specificity for SAHase in *cellulo* was proven by much weaker fluorescence

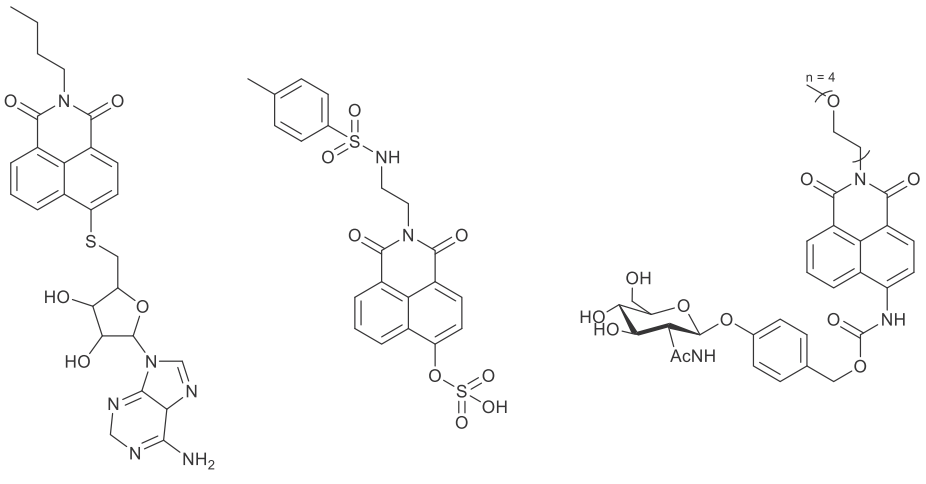

Fig. 42. Chemical structures of compounds **64**–**66**.

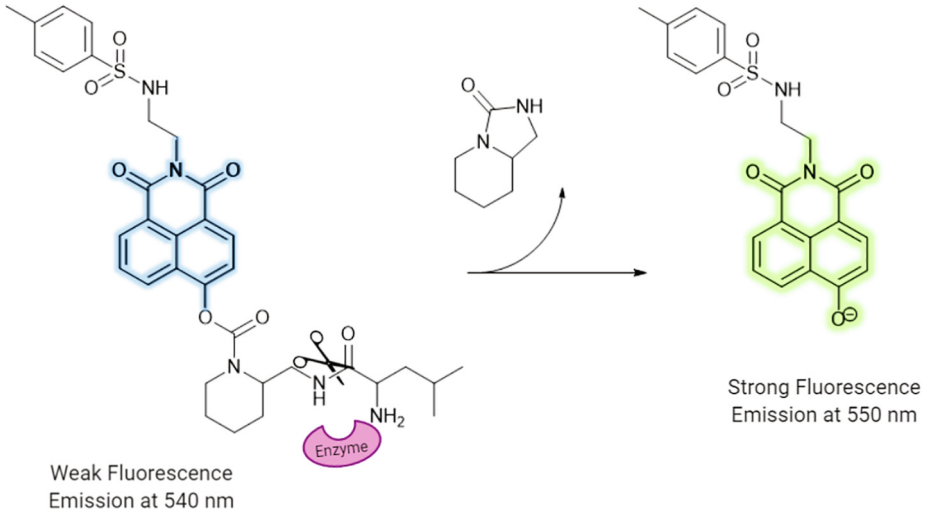

Scheme 20. General schematic for protease cleavage of naphthalimide substrate **60**.

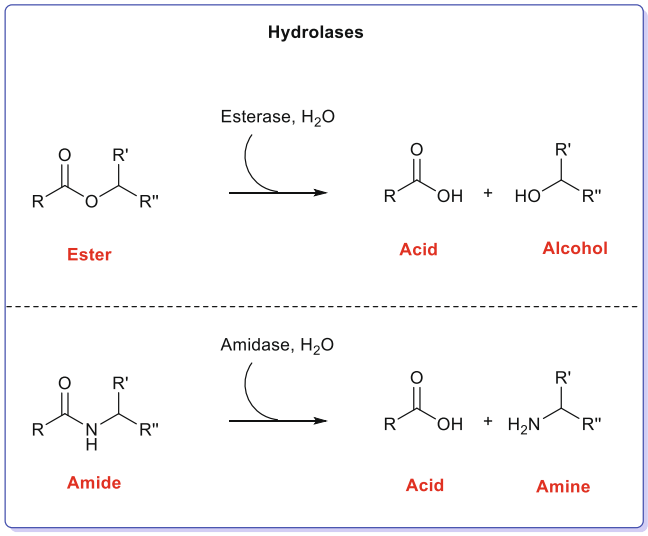

Scheme 21. The hydrolysis of ester and amide bonds in the presence of hydrolases and water.

when HL-60 cells were pre-treated with inhibitor deazaneplanocin-A and by the fact that there was no fluorescence enhancement in the presence of homocysteine.Scheme 22

Another sub-class of hydrolase, steroid sulfatase (STS) has the job of cleaving sulphate from a parent substrate. It is produced predominantly in the endoplasmic reticulum (ER), and the activity of STS has been implicated in numerous types of cancers, among them, oestrogen-related breast cancer [161]. Recently, the group of Xiao Bing and co-workers reported the synthesis of probe **65** to monitor endogenous steroid sulfatase activity (Fig. 42) [162]. The authors were able to achieve detection of STS activity *via* a ratiometric fluorescence response, with enhanced selectivity and sensitivity over commercially available probes. Upon one- and two-photon excitation, **65** exhibited fluorescence signal changes that allowed the assay to differentiate between various cancer cell-types (e.g. oestrogen-dependent) and healthy cells, with tissue-depth penetration of 120 μM. The experimental evidence collected suggests that **65** may pave the way for better STS-related cancer treatment in the future.

Hexosaminidase (Hex) is another biomarker of interest, however, very few fluorescent probes have been engineered to evaluate its activity. One of the most popular fluorescent probes for Hexs is 4-MU-GlcNAc [163], but its metabolite (4-methylumbelliferone) suffers from poor water solubility and no obvious colourimetric change after cleavage [164]. To improve on this, Jianjun and co-workers synthesised an enzyme-activatable fluorescent probe **66**, functionalised with ethylene glycol, and using *N*-acetyl-β-d-glucosaminide as the enzyme substrate (Fig. 42) [165]. Upon activation by Hex, the glucoside linkage of **66** is cleaved rapidly with measurable colourimetric and fluorescent changes (Fig. 43). The fluorescence intensity at 540 nm (**66** + Hex) increases rapidly, effectively eclipsing the emission at 475 nm (**66**), with an isosbestic point at 496 nm. **66** displayed enhanced hydrophilicity and fluorescent characteristics which could be applied to complement the visualisation of intracellular Hexs.

Another recent example reported by Nalder *et al.* detailed the syntheses of 4-Hydroxy-*N*-propyl-1,8-naphthalimide esters **67** – **69** (Fig. 44) as fluorescence probes for the analysis of lipase and esterase activity [166]. The authors showed that each of the esters were stable under a set of representative assay conditions (50 μM probe in 50 mM Tris-HCl, pH 8.0, 0.01% gum arabic, DMSO 0.5% v/v, at 30 °C) with very little spontaneous hydrolysis observed. Moreover, non-specific hydrolysis by proteins such as bovine serum albumin (BSA) was also negligible, particularly for the palmitate based ester **69**. On the other hand, treatment of **67**–**69** with different classes of carboxylester hydrolases, such as lipases and esterases gave rise to varying responses with respect to the hydrolysis of the various chain length esters. Lipases preferentially hydrolysed the medium chain ester **68**, whereas esterases reacted more readily with the shorter ester **67**. In all cases, an increase in fluorescence (λ_{em} = 555 nm) could be used to quantitatively determine the hydrolysis profiles of the various enzymes and represents a simple and rapid assay to analyse a range of hydrolytic enzymes.

12. Conclusions and outlook

From the above examples it is clear that the 1,8-naphthalimide is a versatile and effective scaffold on which to build fluorescent probes for a wide variety of enzymes. Indeed, the diversity of analytes that have been targeted, and the various

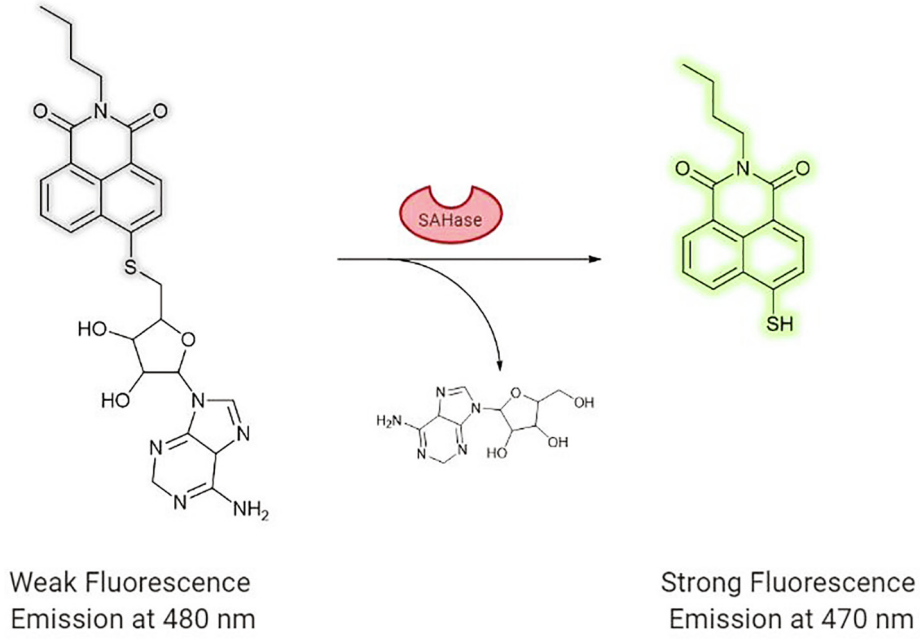

Scheme 22. General schematic for the S-adenosylhomocysteine hydrolase (SAHase) conversion of **64** to 4-thiol substituted naphthalimide.

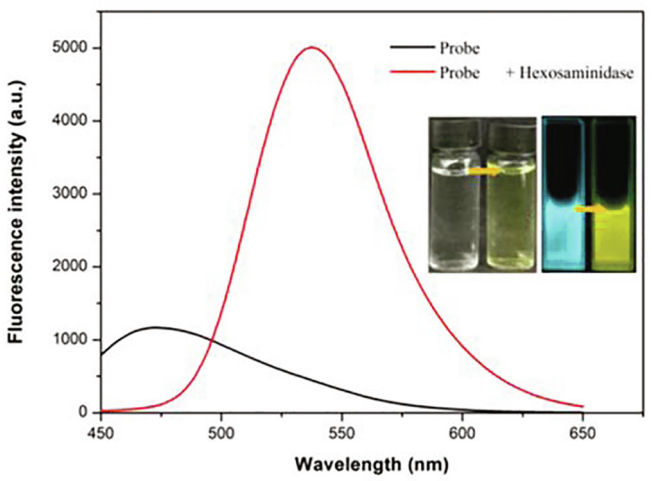

Fig. 43. Fluorescence spectral changes of probe **66** (20×10^{-6} M) with inclusion of Hexs (10×10^{-9} M). Colour/fluorescence change of **66** with and without Hexs. Reprinted with permission from *ACS Sens*. **2019**, 4, (5), 1222–1229, Copyright © 2019, American Chemical Society.

approaches to sensing is a clear demonstration of their utility. While the majority of examples rely on the 'release' of the 4-amino or 4-hydroxy-1,8-naphthalimde structures, new cyclisation approaches and cascade reactions are emerging that also give rise to measurable fluorescent modulations. Indeed, the potential for alternative mechanisms is bolstered by the sheer volume and diversity of enzymatic analytes that exist. Similarly, their cell permeability and sub-cellular localisation characteristics further emphasise the usefulness of 1,8-naphthalimides and reinforce their utility as an effective tool in the study of biological systems, both *in vitro* and *in vivo*. The included examples are just a brief glimpse at the overall possibilities. Future directions may look to focus on reversible bond formations that will allow the measurement of fluxional aspects of cellular environments. For example Pfeffer, New and co-workers have recently reported a fluorescent naphthalimide NADH mimic that allows continuous and reversible sensing of the redox state in a cellular environment [167]. Another likely direction will be the synthesis of naphthalimide based theranostics. Given the known therapeutic ability of several classes of naphthalimides [56,168], probes capable of both detecting a biomarker of interest while simultaneously releasing an active naphthalimide drug will offer obvious advantages. Thirdly, the optimisation of the fluorescence response from new probes will likely be developed in the coming

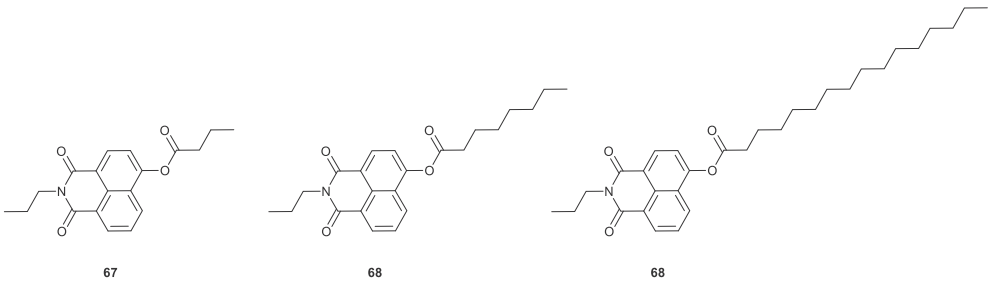

Fig. 44. Chemical structures of compounds **67**–**69**.

years. Some recent examples have shown the ability to shift fluorescence maxima in to the red region of the visible spectrum [169,170]. Lower energy emitters will have obvious advantages for biological tissue penetration, the avoidance of high energy excitation and also show enhanced contrast against autofluorescence. Certainly, with the speed and volume of biomarker discovery and the versatile synthetic methods that are being developed, we can only hope that the reporting of 1,8-naphthalimide based probes for these valuable biomarkers will continue to keep pace.

Declaration of Competing Interest

The authors declare that they have no known competing financial interests or personal relationships that could have appeared to influence the work reported in this paper.

Acknowledgements

The authors would like to acknowledge funding from Science Foundation Ireland (SFI), grant number 12/RC/2275/P2, which is co-funded under the European Regional Development Fund. CG would also like to acknowledge Maynooth University and the Kathleen Lonsdale Institute for Human Health Research for PhD funding.

References

[1] A.P. de Silva, H.Q. Gunaratne, T. Gunnlaugsson, A.J. Huxley, C.P. McCoy, J.T. Rademacher, T.E. Rice, Signaling recognition events with fluorescent sensors and switches, Chem. Rev. 97 (1997) 1515–1566.
[2] D. Wu, A.C. Sedgwick, T. Gunnlaugsson, E.U. Akkaya, J. Yoon, T.D. James, Fluorescent chemosensors: the past, present and future, Chem. Soc. Rev. 46 (2017) 7105–7123.
[3] S. Lee, K.K.Y. Yuen, K.A. Jolliffe, J. Yoon, Fluorescent and colorimetric chemosensors for pyrophosphate, Chem. Soc. Rev. 44 (2015) 1749–1762.
[4] P.D. Beer, P.A. Gale, Anion recognition and sensing: the state of the art and future perspectives, Angew. Chem. Int. Ed. 40 (2001) 486–516.
[5] S.D. Bull, M.G. Davidson, J.M. van den Elsen, J.S. Fossey, A.T. Jenkins, Y.B. Jiang, Y. Kubo, F. Marken, K. Sakurai, J. Zhao, T.D. James, Exploiting the reversible covalent bonding of boronic acids: recognition, sensing, and assembly, Acc. Chem. Res. 46 (2013) 312–326.
[6] W. Chyan, R.T. Raines, Enzyme-activated fluorogenic probes for live-cell and in vivo imaging, ACS Chem. Biol. 13 (2018) 1810–1823.
[7] H. Kobayashi, M. Ogawa, R. Alford, P.L. Choyke, Y. Urano, New strategies for fluorescent probe design in medical diagnostic imaging, Chem. Rev. 110 (2010) 2620–2640.
[8] X. Chen, T. Pradhan, F. Wang, J.S. Kim, J. Yoon, Fluorescent chemosensors based on spiroring-opening of xanthenes and related derivatives, Chem. Rev. 112 (2012) 1910–1956.
[9] X. Li, X. Gao, W. Shi, H. Ma, Design strategies for water-soluble small molecular chromogenic and fluorogenic probes, Chem. Rev. 114 (2014) 590–659.
[10] L. Yuan, W. Lin, K. Zheng, L. He, W. Huang, Far-red to near infrared analyte-responsive fluorescent probes based on organic fluorophore platforms for fluorescence imaging, Chem. Soc. Rev. 42 (2013) 622–661.
[11] J.F. Lovell, T.W. Liu, J. Chen, G. Zheng, Activatable photosensitizers for imaging and therapy, Chem. Rev. 110 (2010) 2839–2857.
[12] D. Asanuma, M. Sakabe, M. Kamiya, K. Yamamoto, J. Hiratake, M. Ogawa, N. Kosaka, P.L. Choyke, T. Nagano, H. Kobayashi, Y. Urano, Sensitive β-galactosidase-targeting fluorescence probe for visualizing small peritoneal metastatic tumours in vivo, Nat. Commun. 6 (2015) 6463.
[13] E. Calatrava-Pérez, S. Acherman, L. Stricker, G. McManus, J. Delente, A.D. Lynes, A.F. Henwood, J.I. Lovitt, C.S. Hawes, K. Byrne, W. Schmitt, O. Kotova, T. Gunnlaugsson, E.M. Scanlan, Fluorescent supramolecular hierarchical self-assemblies from glycosylated 4-amino- and 4-bromo-1,8-naphthalimides, Org. Biomol. Chem. (2020).
[14] T. Fujii, M. Kamiya, Y. Urano, In vivo imaging of intraperitoneally disseminated tumors in model mice by using activatable fluorescent small-molecular probes for activity of cathepsins, Bioconjug. Chem. 25 (2014) 1838–1846.
[15] R.S. Kathayat, P.D. Elvira, B.C. Dickinson, A fluorescent probe for cysteine depalmitoylation reveals dynamic APT signaling, Nat. Chem. Biol. 13 (2017) 150–152.
[16] T.I. Kim, H. Kim, Y. Choi, Y. Kim, A fluorescent turn-on probe for the detection of alkaline phosphatase activity in living cells, Chem. Commun. (Camb.) 47 (2011) 9825–9827.
[17] Z.M. Liu, L. Feng, G.B. Ge, X. Lv, J. Hou, Y.F. Cao, J.N. Cui, L. Yang, A highly selective ratiometric fluorescent probe for in vitro monitoring and cellular imaging of human carboxylesterase 1, Biosens. Bioelectron. 57 (2014) 30–35.
[18] M. Sakabe, D. Asanuma, M. Kamiya, R.J. Iwatate, K. Hanaoka, T. Terai, T. Nagano, Y. Urano, Rational design of highly sensitive fluorescence probes for protease and glycosidase based on precisely controlled spirocyclization, J. Am. Chem. Soc. 135 (2013) 409–414.
[19] H. Shi, R.T. Kwok, J. Liu, B. Xing, B.Z. Tang, B. Liu, Real-time monitoring of cell apoptosis and drug screening using fluorescent light-up probe with aggregation-induced emission characteristics, J. Am. Chem. Soc. 134 (2012) 17972–17981.
[20] X. Ao, S.A. Bright, N.C. Taylor, R.B.P. Elmes, 2-Nitroimidazole based fluorescent probes for nitroreductase; monitoring reductive stress in cellulo, Org. Biomol. Chem. 15 (2017) 6104–6108.
[21] Z.R. Dai, G.B. Ge, L. Feng, J. Ning, L.H. Hu, Q. Jin, D.D. Wang, X. Lv, T.Y. Dou, J.N. Cui, L. Yang, A Highly Selective Ratiometric Two-Photon Fluorescent Probe for Human Cytochrome P450 1A, J. Am. Chem. Soc. 137 (2015) 14488–14495.
[22] T.I. Kim, J. Park, S. Park, Y. Choi, Y. Kim, Visualization of tyrosinase activity in melanoma cells by a BODIPY-based fluorescent probe, Chem. Commun. (Camb.) 47 (2011) 12640–12642.
[23] L. Li, C.W. Zhang, G.Y. Chen, B. Zhu, C. Chai, Q.H. Xu, E.K. Tan, Q. Zhu, K.L. Lim, S.Q. Yao, A sensitive two-photon probe to selectively detect monoamine oxidase B activity in Parkinson's disease models, Nat. Commun. 5 (2014) 3276.
[24] L. Zhang, D. Duan, Y. Liu, C. Ge, X. Cui, J. Sun, J. Fang, Highly selective off-on fluorescent probe for imaging thioredoxin reductase in living cells, J. Am. Chem. Soc. 136 (2014) 226–233.
[25] G. Blum, G. von Degenfeld, M.J. Merchant, H.M. Blau, M. Bogyo, Noninvasive optical imaging of cysteine protease activity using fluorescently quenched activity-based probes, Nat. Chem. Biol. 3 (2007) 668–677.
[26] A. Cobos-Correa, J.B. Trojanek, S. Diemer, M.A. Mall, C. Schultz, Membrane-bound FRET probe visualizes MMP12 activity in pulmonary inflammation, Nat. Chem. Biol. 5 (2009) 628–630.
[27] K. Kiyose, K. Hanaoka, D. Oushiki, T. Nakamura, M. Kajimura, M. Suematsu, H. Nishimatsu, T. Yamane, T. Terai, Y. Hirata, T. Nagano, Hypoxia-sensitive fluorescent probes for in vivo real-time fluorescence imaging of acute ischemia, J. Am. Chem. Soc. 132 (2010) 15846–15848.
[28] L. Li, J. Ge, H. Wu, Q.H. Xu, S.Q. Yao, Organelle-specific detection of phosphatase activities with two-photon fluorogenic probes in cells and tissues, J. Am. Chem. Soc. 134 (2012) 12157–12167.
[29] J. Mu, F. Liu, M.S. Rajab, M. Shi, S. Li, C. Goh, L. Lu, Q.H. Xu, B. Liu, L.G. Ng, B. Xing, A small-molecule FRET reporter for the real-time visualization of cell-surface proteolytic enzyme functions, Angew. Chem., Int. Ed. Engl. 53 (2014) 14357–14362.
[30] A.K. Yadav, D.L. Shen, X. Shan, X. He, A.R. Kermode, D.J. Vocadlo, Fluorescence-quenched substrates for live cell imaging of human glucocerebrosidase activity, J. Am. Chem. Soc. 137 (2015) 1181–1189.
[31] A. Podder, S.M. Alex, M. Maiti, K.K. Maiti, S. Bhuniya, Self-calibrated fluorescent probe resembled as an indicator of the lysosomal phosphatase pertaining to the cancer cells, J. Photochem. Photobiol. B 177 (2017) 105–111.
[32] J. Zhou, W. Shi, L.-H. Li, Q.-Y. Gong, X.-F. Wu, X.-H. Li, H.-M. Ma, A lysosome-targeting fluorescence off-on probe for imaging of nitroreductase and hypoxia in live cells, Chem. Asian J. 11 (2016) 2719–2724.
[33] W.C. Silvers, B. Prasai, D.H. Burk, M.L. Brown, R.L. McCarley, Profluorogenic reductase substrate for rapid, selective, and sensitive visualization and detection of human cancer cells that overexpress NQO1, J. Am. Chem. Soc. 135 (2013) 309–314.
[34] M.H. Lee, J.S. Kim, J.L. Sessler, Small molecule-based ratiometric fluorescence probes for cations, anions, and biomolecules, Chem. Soc. Rev. 44 (2015) 4185–4191.
[35] H.W. Liu, L. Chen, C. Xu, Z. Li, H. Zhang, X.B. Zhang, W. Tan, Recent progresses in small-molecule enzymatic fluorescent probes for cancer imaging, Chem. Soc. Rev. 47 (2018) 7140–7180.
[36] B.F. Godley, F.A. Shamsi, F.Q. Liang, S.G. Jarrett, S. Davies, M. Boulton, Blue light induces mitochondrial DNA damage and free radical production in epithelial cells, J. Biol. Chem. 280 (2005) 21061–21066.
[37] R. Weissleder, A clearer vision for in vivo imaging, Nat. Biotechnol. 19 (2001) 316–317.
[38] L. Espinar-Barranco, P. Luque-Navarro, M.A. Strnad, P. Herrero-Foncubierta, L. Crovetto, D. Miguel, M.D. Giron, A. Orte, J.M. Cuerva, R. Salto, J.M. Alvarez-Pez, J.M. Paredes, A solvatofluorochromic silicon-substituted xanthene dye useful in bioimaging, Dyes Pigm. 168 (2019) 264–272.
[39] C. Duan, M. Won, P. Verwilst, J. Xu, H.S. Kim, L. Zeng, J.S. Kim, In vivo imaging of endogenously produced HClO in zebrafish and mice using a bright. Photostable ratiometric fluorescent probe, Anal Chem 91 (2019) 4172–4178.
[40] X. Bao, X. Wu, S.N. Berry, E.N.W. Howe, Y.T. Chang, P.A. Gale, Fluorescent squaramides as anion receptors and transmembrane anion transporters, Chem. Commun. (Camb.) 54 (2018) 1363–1366.
[41] H.N. Kim, M.H. Lee, H.J. Kim, J.S. Kim, J. Yoon, A new trend in rhodamine-based chemosensors: application of spirolactam ring-opening to sensing ions, Chem. Soc. Rev. 37 (2008) 1465–1472.
[42] A. Loudet, K. Burgess, BODIPY Dyes and Their Derivatives: Syntheses and Spectroscopic Properties, Chem. Rev. 107 (2007) 4891–4932.
[43] R.M. Duke, E.B. Veale, F.M. Pfeffer, P.E. Kruger, T. Gunnlaugsson, Colorimetric and fluorescent anion sensors: an overview of recent developments in the use of 1,8-naphthalimide-based chemosensors, Chem. Soc. Rev. 39 (2010) 3936–3953.

[44] S. Banerjee, E.B. Veale, C.M. Phelan, S.A. Murphy, G.M. Tocci, L.J. Gillespie, D.O. Frimannsson, J.M. Kelly, T. Gunnlaugsson, Recent advances in the development of 1,8-naphthalimide based DNA targeting binders, anticancer and fluorescent cellular imaging agents, Chem. Soc. Rev. 42 (2013) 1601–1618.
[45] D. Gudeika, A review of investigation on 4-substituted 1,8-naphthalimide derivatives, Synth. Met. 262 (2020) 116328.
[46] R. Kumari, D. Sunil, R.S. Ningthoujam, Naphthalimides in fluorescent imaging of tumor hypoxia – An up-to-date review, Bioorg. Chem. 88 (2019) 102979.
[47] R.W. Middleton, J. Parrick, E.D. Clarke, P. Wardman, Synthesis and fluorescence of N-substituted-1,8-naphthalimides, J. Heterocycl. Chem. 23 (1986) 849–855.
[48] Y. Fu, N.S. Finney, Small-molecule fluorescent probes and their design, RSC Adv. 8 (2018) 29051–29061.
[49] C.L. Fleming, T.D. Nalder, E.H. Doeven, C.J. Barrow, F.M. Pfeffer, T.D. Ashton, Synthesis of N-substituted 4-hydroxynaphthalimides using palladium-catalysed hydroxylation, Dyes Pigm. 126 (2016) 118–120.
[50] T. Liu, Z. Xu, D.R. Spring, J. Cui, A Lysosome-Targetable Fluorescent Probe for Imaging Hydrogen Sulfide in Living Cells, Org. Lett. 15 (2013) 2310–2313.
[51] S. Chen, P. Hou, J.W. Foley, X. Song, A colorimetric and ratiometric fluorescent probe for Cu2+ with a large red shift and its imaging in living cells, RSC Adv. 3 (2013) 5591–5596.
[52] F.M. Pfeffer, A.M. Buschgens, N.W. Barnett, T. Gunnlaugsson, P.E. Kruger, 4-Amino-1,8-naphthalimide-based anion receptors: employing the naphthalimide N-H moiety in the cooperative binding of dihydrogenphosphate, Tetrahedron Lett. 46 (2005) 6579–6584.
[53] R.M. Duke, T. Gunnlaugsson, Selective fluorescent PET sensing of fluoride (F-) using naphthalimide-thiourea and -urea conjugates, Tetrahedron Lett. 48 (2007) 8043–8047.
[54] H.D.P. Ali, P.E. Kruger, T. Gunnlaugsson, Colorimetric 'naked-eye' and fluorescent sensors for anions based on amidourea functionalised 1,8-naphthalimide structures: anion recognition via either deprotonation or hydrogen bonding in DMSO, New J. Chem. 32 (2008) 1153–1161.
[55] P.A. Panchenko, Y.V. Fedorov, V.P. Perevalov, G. Jonusauskas, O.A. Fedorova, Cation-dependent fluorescent properties of naphthalimide derivatives with N-benzocrown ether fragment, J. Phys. Chem. A 114 (2010) 4118–4122.
[56] M.F. Brana, A. Ramos, Naphthalimides as anti-cancer agents: synthesis and biological activity, Curr. Med. Chem. Anticancer Agents 1 (2001) 237–255.
[57] E.M. Williams, R.F. Little, A.M. Mowday, M.H. Rich, J.V.E. Chan-Hyams, J.N. Copp, J.B. Smaill, A.V. Patterson, D.F. Ackerley, Nitroreductase gene-directed enzyme prodrug therapy: insights and advances toward clinical utility, Biochem. J 471 (2015) 131–153.
[58] W.A. Denny, Prodrug strategies in cancer therapy, Eur. J. Med. Chem. 36 (2001) 577–595.
[59] W.A. Denny, Hypoxia-activated prodrugs in cancer therapy: progress to the clinic, Future Oncol. 6 (2010) 419–428.
[60] K.A. Krohn, J.M. Link, R.P. Mason, Molecular Imaging of Hypoxia, J. Nucl. Med. 49 (2008) 129S–148S.
[61] J. Pacheco-Torres, P. López-Larrubia, P. Ballesteros, S. Cerdán, Imaging tumor hypoxia by magnetic resonance methods, NMR Biomed. 24 (2011) 1–16.
[62] Y. Liu, Y. Xu, X. Qian, J. Liu, L. Shen, J. Li, Y. Zhang, Novel fluorescent markers for hypoxic cells of naphthalimides with two heterocyclic side chains for bioreductive binding, Bioorg. Med. Chem. 14 (2006) 2935–2941.
[63] M. Dai, W. Zhu, Y. Xu, X. Qian, Y. Liu, Y. Xiao, Y. You, Versatile nitro-fluorophore as highly effective sensor for hypoxic tumor cells: design, imaging and evaluation, J. Fluores. 18 (2008) 591–597.
[64] H. Yin, W. Zhu, Y. Xu, M. Dai, X. Qian, Y. Li, J. Liu, Novel aliphatic N-oxide of naphthalimides as fluorescent markers for hypoxic cells in solid tumor, Eur. J. Med. Chem. 46 (2011) 3030–3037.
[65] L. Cui, Y. Zhong, W. Zhu, Y. Xu, Q. Du, X. Wang, X. Qian, Y. Xiao, A new prodrug-derived ratiometric fluorescent probe for hypoxia: high selectivity of nitroreductase and imaging in tumor cell, Org. Lett. 13 (2011) 928–931.
[66] Z. He, Y. Chou, H. Zhou, H. Zhang, T. Cheng, G. Liu, A nitroreductase and acidity detecting dual functional ratiometric fluorescent probe for selectively imaging tumor cells, Org. Biomol. Chem. 16 (2018) 3266–3272.
[67] Y. Fang, W. Shi, Y. Hu, X. Li, H. Ma, A dual-function fluorescent probe for monitoring the degrees of hypoxia in living cells via the imaging of nitroreductase and adenosine triphosphate, Chem. Commun. 54 (2018) 5454–5457.
[68] Z. Zhang, T. Lv, B. Tao, Z. Wen, Y. Xu, H. Li, F. Liu, S. Sun, A novel fluorescent probe based on naphthalimide for imaging nitroreductase (NTR) in bacteria and cells, Bioorg. Med. Chem. 28 (2020) 115280.
[69] C. Wei, Y. Shen, Z. Xu, S. Peng, Z. Yuan, Y. He, J. Yin, H. Chen, A novel off-on fluorescent probe for imaging of hypoxia in tumor cell, J. Photochem. Photobiol., A 353 (2018) 292–298.
[70] A. Xu, Y. Tang, W. Lin, Endoplasmic reticulum-targeted two-photon turn-on fluorescent probe for nitroreductase in tumor cells and tissues, Spectrochim. Acta. A 204 (2018) 770–776.
[71] K.G. Leslie, D. Jacquemin, E.J. New, K.A. Jolliffe, Expanding the Breadth of 4-Amino-1,8-naphthalimide Photophysical Properties through Substitution of the Naphthalimide Core, Chem. Eur. J. 24 (2018) 5569–5573.
[72] K. Yang, K.G. Leslie, S.Y. Kim, B. Kalionis, W. Chrzanowski, K.A. Jolliffe, E.J. New, Tailoring the properties of a hypoxia-responsive 1,8-naphthalimide for imaging applications, Org. Biomol. Chem. 16 (2018) 619–624.
[73] L.D. Adair, N. Trinh, P.M. Vérité, D. Jacquemin, K.A. Jolliffe, E.J. New, Synthesis of nitro-aryl functionalised 4-amino-1,8-naphthalimides and their evaluation as fluorescent hypoxia sensors, Chem. Eur. J. 26 (2020) 10064–10071.
[74] Z. Zhang, Q. Feng, M. Yang, Y. Tang, A ratiometric fluorescent biosensor based on conjugated polymers for sensitive detection of nitroreductase and hypoxia diagnosis in tumor cells, Sens. Actuators, B 318 (2020) 128257.
[75] L. Ernster, F. Navazio, Soluble diaphorase in animal tissues, Acta Chem. Scand. 12 (1958) 595.
[76] M. Nakamura, T. Hayashi, One- and two-electron reduction of quinones by rat liver subcellular fractions, J. Biochem. 115 (1994) 1141–1147.
[77] L. Ernster, [56] DT diaphorase, Methods in Enzymology, Vol. 10, Academic Press, 1967, pp. 309–317.
[78] A.T. Dinkova-Kostova, P. Talalay, NAD(P)H:quinone acceptor oxidoreductase 1 (NQO1), a multifunctional antioxidant enzyme and exceptionally versatile cytoprotector, Arch. Biochem. Biophys. 501 (2010) 116–123.
[79] S. Danson, T.H. Ward, J. Butler, M. Ranson, DT-diaphorase: a target for new anticancer drugs, Cancer Treat. Rev. 30 (2004) 437–449.
[80] X. Cui, L. Li, G. Yan, K. Meng, Z. Lin, Y. Nan, G. Jin, C. Li, High expression of NQO1 is associated with poor prognosis in serous ovarian carcinoma, BMC Cancer 15 (2015), 244-244.
[81] Y. Chen, L. Hu, Design of anticancer prodrugs for reductive activation, Med. Res. Rev. 29 (2009) 29–64.
[82] Lakowicz, J. R.: Principles of fluorescence spectroscopy, 2006.
[83] S.U. Hettiarachchi, B. Prasai, R.L. McCarley, Detection and cellular imaging of human cancer enzyme using a turn-on, wavelength-shiftable, self-immolative profluorophore, J. Am. Chem. Soc. 136 (2014) 7575–7578.
[84] B. Prasai, W.C. Silvers, R.L. McCarley, Oxidoreductase-facilitated visualization and detection of human cancer cells, Anal. Chem. 87 (2015) 6411–6418.
[85] S.Y. Park, E. Jung, J.S. Kim, S.-G. Chi, M.H. Lee, Cancer-specific hNQO1-responsive biocompatible naphthalimides providing a rapid fluorescent turn-on with an enhanced enzyme affinity, Sensors 20 (2020).
[86] S.Y. Park, M. Won, C. Kang, J.S. Kim, M.H. Lee, A coumarin-naphthalimide hybrid as a dual emissive fluorescent probe for hNQO1, Dyes Pigm. 164 (2019) 341–345.
[87] W. Cai, L. Zhang, Y. Song, B. Wang, B. Zhang, X. Cui, G. Hu, Y. Liu, J. Wu, J. Fang, Small molecule inhibitors of mammalian thioredoxin reductase, Free Radic Biol Med 52 (2012) 257–265.
[88] J. Lu, A. Holmgren, Thioredoxin system in cell death progression, Antioxid. Redox Signal. 17 (2012) 1738–1747.
[89] M.P. Rigobello, A. Bindoli, Mitochondrial thioredoxin reductase purification, inhibitor studies, and role in cell signaling, Methods Enzymol. 474 (2010) 109–122.
[90] E.S. Arnér, Focus on mammalian thioredoxin reductases–important selenoproteins with versatile functions, BBA 1790 (2009) 495–526.
[91] J. Lu, A. Holmgren, The thioredoxin antioxidant system, Free Radic Biol Med 66 (2014) 75–87.
[92] A. Holmgren, J. Lu, Thioredoxin and thioredoxin reductase: current research with special reference to human disease, Biochem. Biophys. Res. Commun. 396 (2010) 120–124.
[93] Y. Liu, H. Ma, L. Zhang, Y. Cui, X. Liu, J. Fang, A small molecule probe reveals declined mitochondrial thioredoxin reductase activity in a Parkinson's disease model, Chem. Commun. 52 (2016) 2296–2299.
[94] L. Zhang, D. Duan, Y. Liu, C. Ge, X. Cui, J. Sun, J. Fang, Highly selective off–on fluorescent probe for imaging thioredoxin reductase in living cells, J. Am. Chem. Soc. 136 (2014) 226–233.
[95] J. Singh Sidhu, A. Singh, N. Garg, N. Kaur, N. Singh, A highly selective naphthalimide-based ratiometric fluorescent probe for the recognition of tyrosinase and cellular imaging, Analyst 143 (2018) 4476–4483.
[96] J. Zhou, W. Shi, L. Li, Q. Gong, X. Wu, X. Li, H. Ma, Detection of misdistribution of tyrosinase from melanosomes to lysosomes and its upregulation under psoralen/ultraviolet a with a melanosome-targeting tyrosinase fluorescent probe, Anal. Chem. 88 (2016) 4557–4564.
[97] S. Zolghadri, A. Bahrami, M.T. Hassan Khan, J. Munoz-Munoz, F. Garcia-Molina, F. Garcia-Canovas, A.A. Saboury, A comprehensive review on tyrosinase inhibitors, J. Enzyme Inhib. Med. Chem. 34 (2019) 279–309.
[98] J.P. Finberg, J.M. Rabey, Inhibitors of MAO-A and MAO-B in psychiatry and neurology, Front. Pharmacol. 7 (2016) 340.
[99] X. Wu, L. Li, W. Shi, Q. Gong, X. Li, H. Ma, Sensitive and selective ratiometric fluorescence probes for detection of intracellular endogenous monoamine oxidase A, Anal. Chem. 88 (2016) 1440–1446.
[100] Z. Meng, L. Yang, C. Yao, H. Li, Y. Fu, K. Wang, Z. Qu, Z. Wang, Development of a naphthlimide-based fluorescent probe for imaging monoamine oxidase A in living cells and zebrafish, Dyes Pigm. 176 (2020) 108208.
[101] X. Zhang, Y. Zhou, X. Gu, Y. Cheng, M. Hong, L. Yan, F. Ma, Z. Qi, Synthesis of a selective ratiometric fluorescent probe based on Naphthalimide and its application in human cytochrome P450 1A, Talanta 186 (2018) 413–420.
[102] C. Zhang, A.M. Ren, J.F. Guo, D. Wang, L.Y. Yu, Theoretical design and investigation of 1,8-naphthalimide-based two-photon fluorescent probes for detecting cytochrome P450 1A with separated fluorescence signal, PCCP 20 (2018) 13290–13305.
[103] Z.-R. Dai, L. Feng, Q. Jin, H. Cheng, Y. Li, J. Ning, Y. Yu, G.-B. Ge, J.-N. Cui, L. Yang, A practical strategy to design and develop an isoform-specific fluorescent probe for a target enzyme: CYP1A1 as a case study, Chem. Sci. 8 (2017) 2795–2803.

[104] L.F. Tietze, J.M. von Hof, M. Müller, B. Krewer, I. Schuberth, Glycosidic prodrugs of highly potent bifunctional duocarmycin derivatives for selective treatment of cancer, Angew. Chem. Int. Ed. 49 (2010) 7336–7339.
[105] I. Tranoy-Opalinski, T. Legigan, R. Barat, J. Clarhaut, M. Thomas, B. Renoux, S. Papot, β-Glucuronidase-responsive prodrugs for selective cancer chemotherapy: An update, Eur. J. Med. Chem. 74 (2014) 302–313.
[106] D.R. Friend, G.W. Chang, A colon-specific drug-delivery system based on drug glycosides and the glycosidases of colonic bacteria, J. Med. Chem. 27 (1984) 261–266.
[107] E.C. Calvaresi, P.J. Hergenrother, Glucose conjugation for the specific targeting and treatment of cancer, Chem. Sci. 4 (2013) 2319–2333.
[108] E. Calatrava-Pérez, S.A. Bright, S. Achermann, C. Moylan, M.O. Senge, E.B. Veale, D.C. Williams, T. Gunnlaugsson, E.M. Scanlan, Glycosidase activated release of fluorescent 1,8-naphthalimide probes for tumor cell imaging from glycosylated 'pro-probes', Chem. Commun. 52 (2016) 13086–13089.
[109] B. Sperker, J.T. Backman, H.K. Kroemer, The role of β-glucuronidase in drug disposition and drug targeting in humans, Clin. Pharmacokinet. 33 (1997) 18–31.
[110] S.J. Pellock, M.R. Redinbo, Glucuronides in the gut: Sugar-driven symbioses between microbe and host, J. Biol. Chem. 292 (2017) 8569–8576.
[111] X. Huo, X. Tian, Y. Li, L. Feng, Y. Cui, C. Wang, J. Cui, C. Sun, K. Liu, X. Ma, A highly selective ratiometric fluorescent probe for real-time imaging of β-glucuronidase in living cells and zebrafish, Sens. Actuators, B 262 (2018) 508–515.
[112] D.H. Juers, B.W. Matthews, R.E. Huber, LacZ β-galactosidase: Structure and function of an enzyme of historical and molecular biological importance, Protein Sci. 21 (2012) 1792–1807.
[113] S.K. Chatterjee, J.J. Barlow, Glycosyltransferase and glycosidase activities in ovarian cancer patients, Cancer Res. 39 (1979) 1943–1951.
[114] G.P. Dimri, X. Lee, G. Basile, M. Acosta, G. Scott, C. Roskelley, E.E. Medrano, M. Linskens, I. Rubelj, O. Pereira-Smith, et al., A biomarker that identifies senescent human cells in culture and in aging skin in vivo, PNAS 92 (1995) 9363–9367.
[115] X. Chen, X. Ma, Y. Zhang, G. Gao, J. Liu, X. Zhang, M. Wang, S. Hou, Ratiometric fluorescent probes with a self-immolative spacer for real-time detection of β-galactosidase and imaging in living cells, Anal. Chim. Acta 1033 (2018) 193–198.
[116] E. Calatrava-Pérez, J.M. Delente, S. Shanmugaraju, C.S. Hawes, C.D. Williams, T. Gunnlaugsson, E.M. Scanlan, Glycosylated naphthalimides and naphthalimide Tröger's bases as fluorescent aggregation probes for Con A, Org. Biomol. Chem. 17 (2019) 2116–2125.
[117] J. Huang, N. Li, Q. Wang, Y. Gu, P. Wang, A lysosome-targetable and two-photon fluorescent probe for imaging endogenous β-galactosidase in living ovarian cancer cells, Sens. Actuators, B 246 (2017) 833–839.
[118] B. Lozano-Torres, I. Galiana, M. Rovira, E. Garrido, S. Chaib, A. Bernardos, D. Muñoz-Espín, M. Serrano, R. Martínez-Máñez, F. Sancenón, An OFF–ON two-photon fluorescent probe for tracking cell senescence in vivo, J. Am. Chem. Soc. 139 (2017) 8808–8811.
[119] C. Guillemette, É. Lévesque, M. Rouleau, Pharmacogenomics of human uridine diphospho-glucuronosyltransferases and clinical implications, Clin. Pharmacol. Ther. 96 (2014) 324–339.
[120] A. Rowland, J.O. Miners, P.I. Mackenzie, The UDP-glucuronosyltransferases: their role in drug metabolism and detoxification, Int. J. Biochem. Cell Biol. 45 (2013) 1121–1132.
[121] T.K. Kiang, M.H. Ensom, T.K. Chang, UDP-glucuronosyltransferases and clinical drug-drug interactions, Pharmacol. Ther. 106 (2005) 97–132.
[122] K.W. Bock, Roles of human UDP-glucuronosyltransferases in clearance and homeostasis of endogenous substrates, and functional implications, Biochem. Pharmacol. 96 (2015) 77–82.
[123] J.D. Hayes, J.U. Flanagan, I.R. Jowsey, Glutathione transferases, Annu. Rev. Pharmacol. Toxicol. 45 (2004) 51–88.
[124] G.J. Beckett, B.J. Chapman, E.H. Dyson, J.D. Hayes, Plasma glutathione S-transferase measurements after paracetamol overdose: evidence for early hepatocellular damage, Gut 26 (1985) 26–31.
[125] C.D. Illio, G.D. Boccio, A. Aceto, R. Casaccia, F. Mucilli, G. Federici, Elevation of glutathione transferase activity in human lung tumor, Carcinogenesis 9 (1988) 335–340.
[126] M. Tatematsu, H. Tsuda, T. Shirai, T. Masui, N. Ito, Placental glutathione S-transferase (GST-P) as a new marker for hepatocarcinogenesis. In vivo short-term screening for hepatocarcinogens, Toxicol. Pathol. 15 (1987) 60–68.
[127] X. Lv, G.-B. Ge, L. Feng, J. Troberg, L.-H. Hu, J. Hou, H.-L. Cheng, P. Wang, Z.-M. Liu, M. Finel, J.-N. Cui, L. Yang, An optimized ratiometric fluorescent probe for sensing human UDP-glucuronosyltransferase 1A1 and its biological applications, Biosens. Bioelectron. 72 (2015) 261–267.
[128] X. Lv, L. Feng, C.-Z. Ai, J. Hou, P. Wang, L.-W. Zou, J. Cheng, G.-B. Ge, J.-N. Cui, L. Yang, A practical and high-affinity fluorescent probe for uridine diphosphate glucuronosyltransferase 1A1: A good surrogate for bilirubin, J. Med. Chem. 60 (2017) 9664–9675.
[129] J. Zhang, Z. Jin, X.-X. Hu, H.-M. Meng, J. Li, X.-B. Zhang, H.-W. Liu, T. Deng, S. Yao, L. Feng, Efficient two-photon fluorescent probe for glutathione s-transferase detection and imaging in drug-induced liver injury sample, Anal. Chem. 89 (2017) 8097–8103.
[130] Y. Fujikawa, K. Terakado, T. Nampo, M. Mori, H. Inoue, 4-Bromo-1,8-naphthalimide derivatives as fluorogenic substrates for live cell imaging of glutathione S-transferase (GST) activity, Talanta 204 (2019) 633–640.
[131] L. Feng, P. Li, J. Hou, Y.-L. Cui, X.-G. Tian, Z.-L. Yu, J.-N. Cui, C. Wang, X.-K. Huo, J. Ning, X.-C. Ma, Identification and isolation of glucosytransferases (GT) expressed fungi using a two-photon ratiometric fluorescent probe activated by GT, Anal. Chem. 90 (2018) 13341–13347.
[132] L. Feng, Q. Yan, B. Zhang, X. Tian, C. Wang, Z. Yu, J. Cui, D. Guo, X. Ma, T.D. James, Ratiometric fluorescent probe for sensing Streptococcus mutans glucosyltransferase, a key factor in the formation of dental caries, Chem. Commun. 55 (2019) 3548–3551.
[133] A. Pompella, V. De Tata, A. Paolicchi, F. Zunino, Expression of gamma-glutamyltransferase in cancer cells and its significance in drug resistance, Biochem. Pharmacol. 71 (2006) 231–238.
[134] H. Zhang, K. Wang, X. Xuan, Q. Lv, Y. Nie, H. Guo, Cancer cell-targeted two-photon fluorescence probe for the real-time ratiometric imaging of DNA damage, Chem. Commun. (Camb.) 52 (2016) 6308–6311.
[135] Y. Urano, M. Sakabe, N. Kosaka, M. Ogawa, M. Mitsunaga, D. Asanuma, M. Kamiya, M.R. Young, T. Nagano, P.L. Choyke, H. Kobayashi, Rapid cancer detection by topically spraying a γ-glutamyltranspeptidase-activated fluorescent probe, Sci. Transl. Med. 3 (2011) 110ra119.
[136] H. Tong, Y. Zheng, L. Zhou, X. Li, R. Qian, R. Wang, J. Zhao, K. Lou, W. Wang, Enzymatic cleavage and subsequent facile intramolecular transcyclization for in situ fluorescence detection of γ-glutamyltranspetidase activities, Anal. Chem. 88 (2016) 10816–10820.
[137] J.E. Coleman, Structure and mechanism of alkaline phosphatase, Annu. Rev. Biophys. Biomol. Struct. 21 (1992) 441–483.
[138] P.L. Wolf, Clinical significance of serum high-molecular-mass alkaline phosphatase, alkaline phosphatase–lipoprotein-X complex, and intestinal variant alkaline phosphatase, J. Clin. Lab. Anal. 8 (1994) 172–176.
[139] K. Ooi, K. Shiraki, Y. Morishita, T. Nobori, High-molecular intestinal alkaline phosphatase in chronic liver diseases, J. Clin. Lab. Anal. 21 (2007) 133–139.
[140] R.E. Gyurcsányi, A. Bereczki, G. Nagy, M.R. Neuman, E. Lindner, Amperometric microcells for alkaline phosphatase assay, Analyst 127 (2002) 235–240.
[141] F. Ma, W.-J. Liu, L. Liang, B. Tang, C.-Y. Zhang, Sensitive detection of alkaline phosphatase by dephosphorylation-initiated transcription reaction-mediated dual signal amplification, Chem. Commun. 54 (2018) 2413–2416.
[142] L.-J. Wang, Z.-Y. Wang, C.-Y. Zhang, Primer dephosphorylation-initiated circular exponential amplification for ultrasensitive detection of alkaline phosphatase, Analyst 143 (2018) 4606–4613.
[143] C. Gao, S. Zang, L. Nie, Y. Tian, R. Zhang, J. Jing, X. Zhang, A sensitive ratiometric fluorescent probe for quantitive detection and imaging of alkaline phosphatase in living cells, Anal. Chim. Acta 1066 (2019) 131–135.
[144] I.L.H. Ong, K.L. Yang, Recent developments in protease activity assays and sensors, Analyst 142 (2017) 1867–1881.
[145] R.D. Wilkinson, R. Williams, C.J. Scott, R.E. Burden, Cathepsin S: therapeutic, diagnostic, and prognostic potential, Biol. Chem. 396 (2015) 867–882.
[146] E. Erez, D. Fass, E. Bibi, How intramembrane proteases bury hydrolytic reactions in the membrane, Nature 459 (2009) 371–378.
[147] T. Yogo, K. Umezawa, M. Kamiya, R. Hino, Y. Urano, Development of an activatable fluorescent probe for prostate cancer imaging, Bioconjug. Chem. 28 (2017) 2069–2076.
[148] J.L. Luo, T. Jin, L. Váradi, J.D. Perry, D.E. Hibbs, P.W. Groundwater, Evaluation of fluorogenic aminonaphthalenesulfonamides and 6-hydrazinobenz[de] isoquinoline-1,3-diones for the detection of bacteria, Dyes Pigm. 125 (2016) 15–26.
[149] Y. Chen, J. Cao, X. Jiang, Z. Pan, N. Fu, A sensitive ratiometric fluorescence probe for chymotrypsin activity and inhibitor screening, Sens. Actuators, B 273 (2018) 204–210.
[150] D. Fruci, S. Ferracuti, M.Z. Limongi, V. Cunsolo, E. Giorda, R. Fraioli, L. Sibilio, O. Carroll, A. Hattori, P.M. van Endert, P. Giacomini, Expression of endoplasmic reticulum aminopeptidases in EBV-B cell lines from healthy donors and in leukemia/lymphoma, carcinoma, and melanoma cell lines, J. Immunol. 176 (2006) 4869–4879.
[151] S. Xu, H.W. Liu, X.X. Hu, S.Y. Huan, J. Zhang, Y.C. Liu, L. Yuan, F.L. Qu, X.B. Zhang, W. Tan, Visualization of endoplasmic reticulum aminopeptidase 1 under different redox conditions with a two-photon fluorescent probe, Anal. Chem. 89 (2017) 7641–7648.
[152] R.E. Wang, Y. Niu, H. Wu, Y. Hu, J. Cai, Development of NGR-based anti-cancer agents for targeted therapeutics and imaging, Anticancer Agents Med. Chem. 12 (2012) 76–86.
[153] N. Haraguchi, H. Ishii, K. Mimori, F. Tanaka, M. Ohkuma, H.M. Kim, H. Akita, D. Takiuchi, H. Hatano, H. Nagano, G.F. Barnard, Y. Doki, M. Mori, CD13 is a therapeutic target in human liver cancer stem cells, J Clin Invest 120 (2010) 3326–3339.
[154] L. Chen, W. Sun, J. Li, Z. Liu, Z. Ma, W. Zhang, L. Du, W. Xu, H. Fang, M. Li, The first ratiometric fluorescent probes for aminopeptidase N cell imaging, Org. Biomol. Chem. 11 (2013) 378–382.
[155] F. Kikkawa, K. Ino, H. Kajiyama, K. Shibata, S. Nomura, S. Mizutani, 26 – role of immunohistochemical expression of aminopeptidases in ovarian carcinoma, in: M.A. Hayat (Ed.), Handbook of Immunohistochemistry and in Situ Hybridization of Human Carcinomas, Academic Press, 2006, pp. 509–517.
[156] Group, W. M.-C. R, State of knowledge and data gaps of middle east respiratory syndrome coronavirus (MERS-CoV) in humans, PLoS Curr. 5 (2013).
[157] L.-W. Zou, P. Wang, X.-K. Qian, L. Feng, Y. Yu, D.-D. Wang, Q. Jin, J. Hou, Z.-H. Liu, G.-B. Ge, L. Yang, A highly specific ratiometric two-photon fluorescent probe to detect dipeptidyl peptidase IV in plasma and living systems, Biosens. Bioelectron. 90 (2017) 283–289.

[158] I. Ivanov, D. Tasheva, R. Todorova, M. Dimitrova, Synthesis and use of 4-peptidylhydrazido-N-hexyl-1,8-naphthalimides as fluorogenic histochemical substrates for dipeptidyl peptidase IV and tripeptidyl peptidase I, Eur. J. Med. Chem. 44 (2009) 384–392.
[159] J. Magdalou, S. Fournel-Gigleux, B. Testa, M. Ouzzine, 31 - Biotransformation reactions, in: C.G. Wermuth (Ed.), The Practice of Medicinal Chemistry, second ed., Academic Press, London, 2003, pp. 517–543.
[160] Y. Jia, P. Li, W. Song, G. Zhao, D. Zheng, D. Li, Y. Wang, J. Wang, C. Li, K. Han, Rational design of a profluorescent substrate for S-adenosylhomocysteine hydrolase and its applications in bioimaging and inhibitor screening, ACS Appl. Mater. Interfaces 8 (2016) 25818–25824.
[161] S.R. Hanson, M.D. Best, C.H. Wong, Sulfatases: structure, mechanism, biological activity, inhibition, and synthetic utility, Angew. Chem., Int. Ed. Engl. 43 (2004) 5736–5763.
[162] W. Li, S. Yin, X. Gong, W. Xu, R. Yang, Y. Wan, L. Yuan, X. Zhang, Achieving the ratiometric imaging of steroid sulfatase in living cells and tissues with a two-photon fluorescent probe, Chem. Commun. 56 (2020) 1349–1352.
[163] G.E. Whitworth, M.S. Macauley, K.A. Stubbs, R.J. Dennis, E.J. Taylor, G.J. Davies, I.R. Greig, D.J. Vocadlo, Analysis of PUGNAc and NAG-thiazoline as transition state analogues for human O-GlcNAcase: mechanistic and structural insights into inhibitor selectivity and transition state poise, J. Am. Chem. Soc. 129 (2007) 635–644.
[164] J.A. Mead, J.N. Smith, R.T. Williams, Studies in detoxication. 67. The biosynthesis of the glucuronides of umbelliferone and 4-methylumbelliferone and their use in fluorimetric determination of beta-glucuronidase, Biochem. J. 61 (1955) 569–574.
[165] L. Dong, S. Shen, H. Lu, S. Jin, J. Zhang, Novel glycosylated naphthalimide-based activatable fluorescent probe: A tool for the assessment of hexosaminidase activity and intracellular hexosaminidase imaging, ACS Sens. 4 (2019) 1222–1229.
[166] T.D. Nalder, T.D. Ashton, F.M. Pfeffer, S.N. Marshall, C.J. Barrow, 4-hydroxy-N-propyl-1,8-naphthalimide esters: new fluorescence-based assay for analysing lipase and esterase activity, Biochimie 128–129 (2016) 127–132.
[167] H. Sharma, N.K. Tan, N. Trinh, J.H. Yeo, E.J. New, F.M. Pfeffer, A fluorescent naphthalimide NADH mimic for continuous and reversible sensing of cellular redox state, Chem. Commun. 56 (2020) 2240–2243.
[168] L. Min, X. Hui, Overview of naphthalimide analogs as anticancer agents, Curr. Med. Chem. 16 (2009) 4797–4813.
[169] P.A. Panchenko, M.A. Grin, O.A. Fedorova, M.A. Zakharko, D.A. Pritmov, A.F. Mironov, A.N. Arkhipova, Y.V. Fedorov, G. Jonusauskas, R.I. Yakubovskaya, N. B. Morozova, A.A. Ignatova, A.V. Feofanov, A novel bacteriochlorin–styrylnaphthalimide conjugate for simultaneous photodynamic therapy and fluorescence imaging, PCCP 19 (2017) 30195–30206.
[170] E.E. Rudebeck, R.P. Cox, T.D.M. Bell, R. Acharya, Z. Feng, N. Gueven, T.D. Ashton, F.M. Pfeffer, Mixed alkoxy/hydroxy 1,8-naphthalimides: expanded fluorescence colour palette and in vitro bioactivity, Chem. Commun. 56 (2020) 6866–6869.